ARTICLE

SNX3 drives maturation of *Borrelia* phagosomes by forming a hub for PI(3)P, Rab5a, and galectin-9

Matthias Klose[1], Johann E. Salloum[1], Hannes Gonschior[2], and Stefan Linder[1]

The spirochete *Borrelia burgdorferi*, the causative agent of Lyme disease, is internalized by macrophages and processed in phagolysosomes. Phagosomal compaction, a crucial step in phagolysosome maturation, is driven by contact of Rab5a-positive vesicles with the phagosomal coat. We show that the sorting nexin SNX3 is transported with Rab5a vesicles and that its PX domain enables vesicle–phagosome contact by binding to PI(3)P in the phagosomal coat. Moreover, the C-terminal region of SNX3 recruits galectin-9, a lectin implicated in protein and membrane recycling, which we identify as a further regulator of phagosome compaction. SNX3 thus forms a hub for two distinct vesicle populations, constituting a convergence point for the endosomal recycling machinery, to contribute to phagosome maturation and intracellular processing of borreliae. These data also suggest that the helical shape of *B. burgdorferi* itself, providing sites of high curvature and thus local PI(3)P enrichment at phagosomes, may be one of the driving elements underlying the efficient elimination of spirochetes by immune cells.

Introduction

The spirochete *Borrelia burgdorferi* is the causative agent of Lyme borreliosis (Steere et al., 1977; Burgdorfer et al., 1982), a multisystemic disease affecting primarily the skin, joints, and nervous system of patients (Zajkowska et al., 2012). Borreliae are characterized by their helical shape and can reach lengths of ≤40 µm (Aberer and Duray, 1991). Borreliae are transferred to a human host through a blood meal by ticks of the *Ixodes* family (Lane and Loye, 1991), and cells of the innate immune system such as neutrophils or macrophages are among the first to encounter infecting borreliae. Successful recognition, uptake, and elimination of borreliae by these cells is thus decisive for the outcome of a respective infection.

Recognition of borreliae by immune cells is mediated by several receptors, including opsonic receptors FcγR (Benach et al., 1984; Montgomery et al., 1994) and CR3 (Cinco et al., 1997; Hawley et al., 2012) and nonoposonic toll-like receptor TLR2 (Salazar et al., 2009), with downstream signaling involving both myeloid differentiation factor 88–dependent and independent pathways (Shin et al., 2009). Capture and immobilization of the highly motile bacteria is initiated through filopodia, cellular protrusions rich in linear actin filaments (Naj et al., 2013; Hoffmann et al., 2014). In a second step, another actin-rich structure, the coiling pseudopod, wraps around the captured bacterium (Rittig et al., 1998).

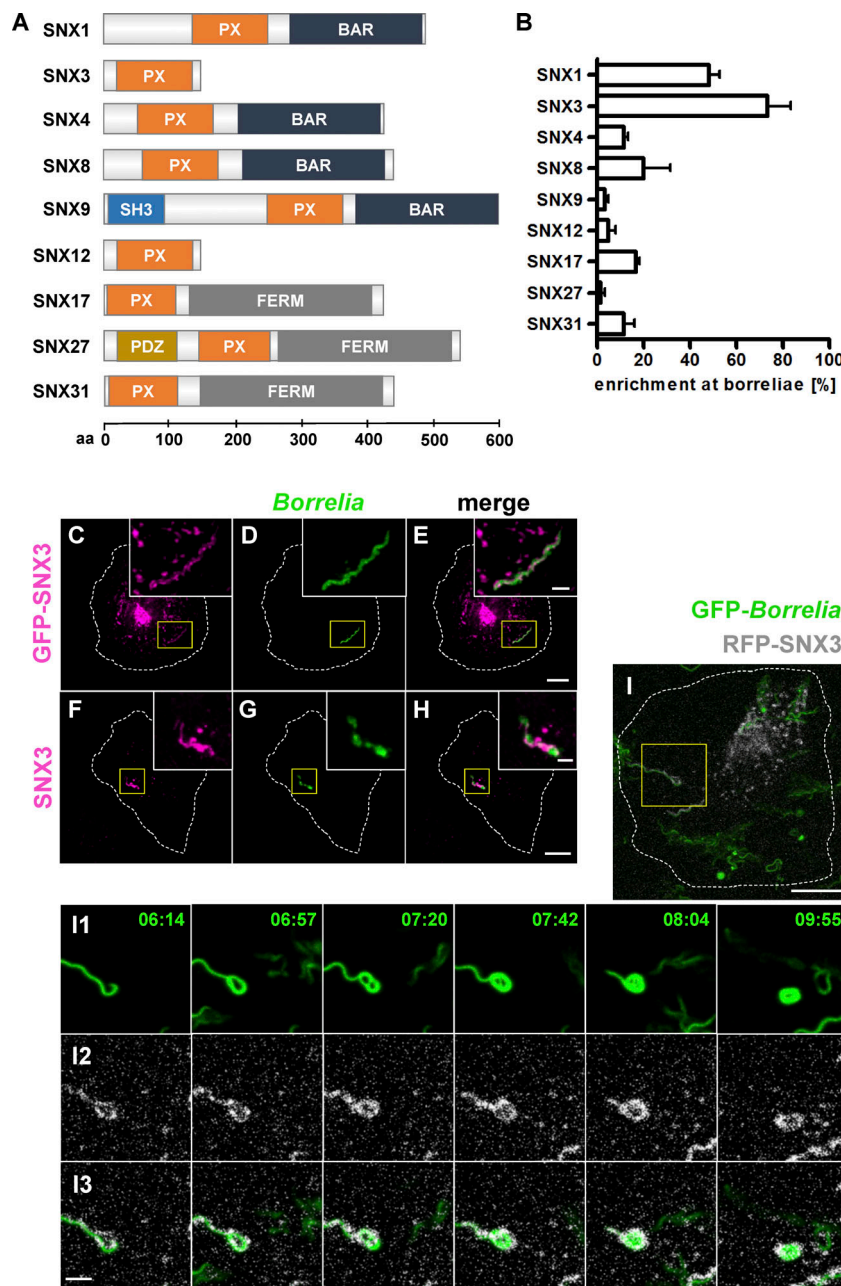Internalization of borreliae by macrophages proceeds through uptake into a phagosomal compartment coated by the RabGTPase Rab22a (Naj and Linder, 2015). Phagosomes are contacted by ER-associated vesicles positive for Rab5a, leading to the formation of membrane tubules, which results in successive reduction of the phagosomal surface and compaction of spirochetes (Naj and Linder, 2015). Phagosomal compaction is a crucial step in the cascade leading to phagolysosome maturation and spirochete breakdown. Accordingly, depletion of either Rab22a or Rab5a leads to reduced phagosome maturation and enhanced intracellular survival of borreliae (Naj and Linder, 2015, 2017). However, the molecular mechanisms that enable docking of Rab5a vesicles to the phagosomal coat are currently unknown.

We now report that Rab5a vesicles carry sorting nexin 3 (SNX3), and that SNX3 binding to phosphoinositol 3-phosphate (PI(3)P), a phospholipid of the phagosomal coat, enables their tethering to borreliae-containing phagosomes. The SNX family comprises a heterologous set of proteins characterized by a phox (PX) domain (Worby and Dixon, 2002), which enables binding to phospholipids, especially PI(3)P and also phosphatidylinositol 4,5-bisphosphate (PI(4,5)P_2; Ponting, 1996; Worby et al., 2001), the former being a central modulator of endosomal trafficking and membrane transport (Simonsen et al., 2001). Minimal isoforms such as SNX3 and SNX12 contain only a PX domain, while a subgroup including, among others, SNX1, SNX4, SNX8, and SNX9 also contains a curvature-sensing/inducing BAR (BIN, amphiphysin, and Rvs167) domain involved in the formation of

Figure 1. **SNX3 localizes to borreliae internalized by macrophages.** **(A)** Domain structure of SNXs. PDZ: PSD95, Dlg1, ZO-1 domain; SH3: Src homology 3 domain. The number of amino acid residues is indicated on the x axis. **(B)** Quantification of enrichment of SNX fusion constructs at internalized borreliae. The number of internalized borreliae was set to 100%. For specific values, see Table S1. n = 3 (3 × 20 borreliae). **(C–H)** Confocal micrographs of macrophages expressing GFP-SNX3 (C–E) or stained for endogenous SNX3 (F–H), with internalized borreliae stained by specific antibody (D and G), and merges (E and H). Box indicates area of magnified insets. Scale bars: 10 μm, and 1 μm for insets. See also Video 1. **(I)** RFP-SNX3 stays associated with compacting borreliae-containing phagosomes. Still images are from confocal time lapse of macrophage with an internalized GFP-expressing *B. burgdorferi* cell (I1) and RFP-SNX3 (shown in white; I2), with merge (I3; see Video 2). Scale bars: 10 μm for overview images and 2 μm for insets. Error bars: mean ± SEM.

membrane tubules (Traer et al., 2007; Cullen and Korswagen, 2011). Another subset including SNX17, SNX27, and SNX31 contains a FERM (protein 4.1, ezrin radixin, moesin) domain enabling β-integrin binding and recycling (Böttcher et al., 2012; Tseng et al., 2014; Fig. 1 A). These features allow individual SNX isoforms to regulate different aspects of endosomal trafficking and membrane recycling, a unifying theme being the binding of phospholipids and the retromer complex (Worby and Dixon, 2002). Accordingly, binding of PI(3)P by SNX3 regulates the morphology of early endosomes and trafficking to recycling endosomes and lysosomes (Xu et al., 2001) and is important for the formation of multivesicular bodies (Pons et al., 2008), while PI(3)P binding by SNX9 regulates actin polymerization at membranes through N-WASP and the Arp2/3 complex (Gallop et al., 2013; Bendris and Schmid, 2017).

Bacterial uptake in immune cells involves significant rearrangements in vesicle trafficking and membrane flow. However, current information on potential roles of SNXs in these processes is limited, with *Salmonella enterica* invasion being the best-studied example. Accordingly, SNX1 organizes a tubular network during establishment of the *Salmonella*-containing vacuole (SCV; Bujny et al., 2008), while depletion of SNX3 leads to reduced formation of *Salmonella*-induced filaments (Braun et al., 2010). Recently, *Chlamydia trachomatis* was shown to hijack SNX5, resulting in disrupted retromer trafficking (Elwell et al., 2017; Paul et al., 2017), whereas SNX10 was found to promote phagosome maturation and protect against infection with *Listeria monocytogenes* (Lou et al., 2017).

We now identify SNX3 as a regulator of phagosomal compaction, phagolysosome maturation, and intracellular processing

of borreliae. siRNA-induced depletion of SNX3 led to a strong reduction in borreliae phagosomal compaction, which was rescued by expression of an siRNA-insensitive WT construct, but not by a mutant defective in PI(3)P binding. SNX3 depletion also led to reduced phagolysosomal maturation and increased intracellular survival of borreliae. Moreover, we identify galectin-9 as an interactor of the SNX3 C-terminus. Galectin-9 is a member of the galectin family that is known to bind carbohydrates on the cell surface but has also emerged as an intracellular regulator of protein and membrane trafficking pathways (Johannes et al., 2018). We now show that galectin-9 functions in the same pathway as SNX3 in borreliae compaction. Collectively, these data indicate that intracellular processing of borreliae is driven by (i) formation of a protein–phospholipid complex through docking of vesicular SNX3 to phagosomal PI(3)P and (ii) recruitment of galectin-9–positive vesicles to phagosomes, thus identifying a crucial connection between membrane recycling pathways and spirochete elimination in human immune cells.

Results

SNX3 regulates phagosomal compaction of borreliae

To identify SNX isoforms potentially involved in membrane recycling from *B. burgdorferi*–containing phagosomes, primary human macrophages were transfected with GFP- or mCherry-fused constructs of nine SNX family members. Isoforms included in the screen were chosen for their documented roles in membrane trafficking (Worby and Dixon, 2002; Carlton et al., 2005; Cullen and Korswagen, 2011) and also for differences in size and domain composition, reflecting the variety of the SNX family (Fig. 1 A). Cells were subsequently coincubated with *B. burgdorferi* spirochetes and stained with antibodies. Localization of SNX fusion proteins at borreliae-containing phagosomes was investigated using confocal microscopy. Strikingly, 73.3% ± 10.1% of borreliae phagosomes showed local enrichments of GFP-SNX3 (Fig. 1, B–E), while GFP-SNX1 was enriched at 48.3% ± 4.4% (Fig. 1 B and Fig. S1, A–C). Fluorescently labeled fusions of SNX4, SNX8, SNX17, and SNX31 were enriched at 12–20% of phagosomes, while respective constructs of SNX9, SNX12, and SNX27 showed enrichments of ≤5% (Fig. 1 B and Fig. S1, D–X). We thus focused in the following on SNX1 and SNX3 as potential regulators of borreliae phagosomal compaction.

Immunofluorescence experiments confirmed the enrichment of endogenous SNX1 (Fig. S2, A and E) and SNX3 (Fig. 1, F–H; and Fig. S2, B and F) at *B. burgdorferi*–containing phagosomes. Interestingly, despite their enrichment at phagosomes, SNX1 and SNX3 did not show extensive colocalization at these structures, suggesting different regulatory roles for these isoforms. Of note, SNX3 was enriched both at elongated and at compacted borreliae (Fig. S2, A–H; and Video 1), while SNX1 was mostly associated only with elongated or partially compacted borreliae (Fig. S2, A–H). Furthermore, live-cell imaging of macrophages coincubated with borreliae showed that GFP-SNX3 becomes enriched early upon internalization of borreliae at respective phagosomes and stays associated with these structures until complete compaction of spirochetes (Fig. 1 I and Video 2). Interestingly, live-cell imaging showed that the majority of GFP-SNX

vesicles were also positive for RFP-Rab5a and that both signals also colocalize at the borreliae phagosomes (Fig. S2 I and Video 3), reminiscent of earlier results of Rab5a-positive vesicles contacting borreliae phagosomes, particularly at sites of high curvature (Naj and Linder, 2015).
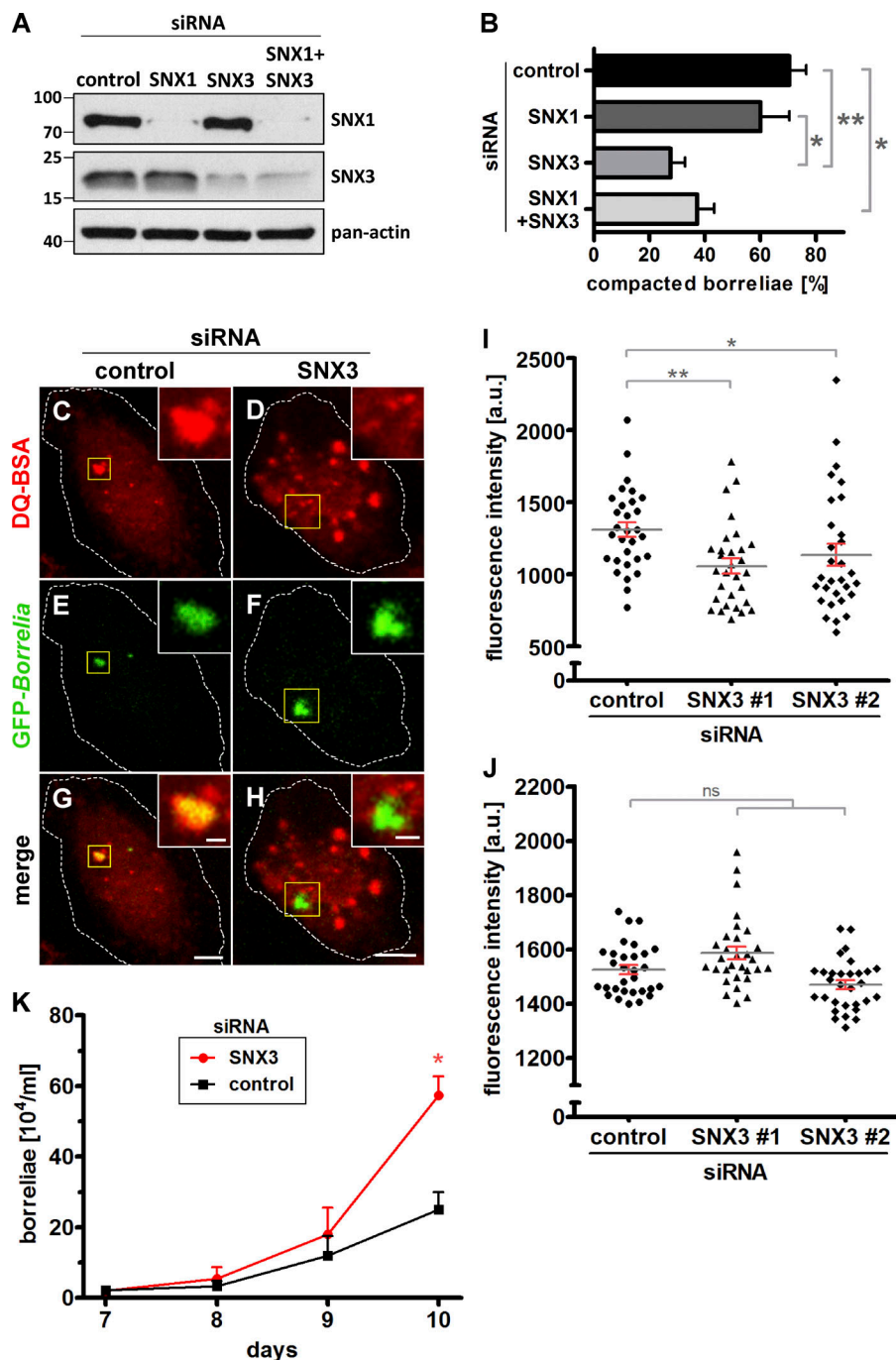
To investigate potential effects of SNX1 and SNX3 on borreliae phagosomal compaction, each time, two individual siRNAs were established. Importantly, siRNA-induced depletion of either SNX isoform did not influence, or only slightly influenced, the protein level of the other isoform (Figs. 2 A and S3), indicating the absence of counterregulatory effects. Compaction of borreliae was assessed in macrophages depleted for SNX1, SNX3, or a combination of both. Depletion of SNX1 led to a slight and not significant reduction of 15% of compaction (60.1% ± 10.4% compaction for SNX1 siRNA–treated cells compared with 70.4% ± 6.2% for controls), while depletion of SNX3 led to a pronounced and highly significant reduction of 61% (27.7% ± 5.3% compaction). Combined knockdown of SNX1 and SNX3 led to a reduction of 47% (37.2% ± 6.2%), comparable to the effect of SNX3 depletion alone (Fig. 2 B). Collectively, these results suggested a role for SNX3, but not SNX1, in phagosomal compaction of borreliae and indicated that SNX3 is present at Rab5a-positive vesicles that contact borreliae phagosomes, especially at sites of high curvature, and becomes progressively enriched at phagosomes during borreliae compaction.

SNX3 is required for proteolytic processing of borreliae

We next investigated whether reduced compaction due to depletion of SNX3 also impacted further maturation of *B. burgdorferi*–containing phagosomes. The proteolytic potential of phagolysosomes was tested by measuring DQ-BSA–based fluorescence in *B. burgdorferi*–containing macrophages. Of note, fluorescence of DQ-BSA is quenched in the intact molecule but becomes apparent upon proteolytic cleavage of the compound (Lee et al., 2005; Naj and Linder, 2015). Macrophages transfected with control siRNA or an SNX3-specific siRNA were coincubated with GFP-expressing borreliae and DQ-BSA and analyzed by confocal microscopy. Compacted borreliae mostly (>90%) colocalized with DQ-BSA signals in control cells (Fig. 2, C, E, and G), while slightly reduced localization of distinct DQ-BSA signals (~70–80%) was observed for borreliae-containing phagosomes (Fig. 2, D, F, and H). Fluorescence measurement showed that SNX3 depletion by two siRNAs led to a reduction of DQ-BSA signals at *B. burgdorferi*–containing phagosomes of 19.3% and 13.4%, respectively, compared with controls (Fig. 2 I). Of note, overall DQ-BSA–based fluorescence was unchanged (Fig. 2 J).

These results suggested that depletion of SNX3 leads to reduced maturation of *B. burgdorferi*–containing phagolysosomes and thus to potentially reduced processing of internalized spirochetes. To test this, macrophages treated with control siRNA or SNX3-specific siRNA were incubated with borreliae for 1 h to allow internalization and uptake into phagosomes. External and adherent spirochetes were subsequently removed by incubation with gentamicin and kanamycin and repeated washing steps (Naj and Linder, 2015). Macrophages were then lysed mechanically, and lysates were conferred to *B. burgdorferi*–specific medium to allow propagation of potentially viable spirochetes. Borreliae could be

Figure 2. **SNX3 regulates phagosomal compaction, proteolytic processing, and intracellular survival of borreliae. (A)** Western blot of lysates from macrophages transfected with control siRNA, SNX1-specific siRNA#1, SNX3-specific siRNA#1, or a combination thereof, developed with SNX1- or SNX3-specific antibodies or pan-actin antibody as loading control. Molecular weight (in kilodaltons) is indicated on the left. **(B)** Evaluation of borreliae compaction in cells treated with control siRNA, SNX1 siRNA#1, SNX3 siRNA#1, or a combination thereof. Values are given as mean ± SEM. For specific values, see Table S1. $n = 3$ (3×30). One-way ANOVA; *, $P < 0.05$; **, $P < 0.01$. **(C–J)** SNX3 regulates proteolytic processing within borreliae-containing phagosomes. **(C–H)** Confocal micrographs of macrophages incubated with DQ-BSA (C and D), to visualize proteolysis, with internalized GFP-expressing borreliae (E and F), with merges (G and H). Macrophages were treated with control siRNA (C, E, and G) or SNX3-specific siRNA (D, F, and H). Scale bars: 10 μm, and 1 μm for insets. **(I and J)** Evaluation of DQ-BSA–based fluorescence intensities at macrophage phagosomes containing (I) or not containing (J) borreliae. Fluorescence intensities are indicated on the y axis. Macrophages were treated with control siRNA or two individual SNX3-specific siRNAs, as indicated. $n = 3$, with DQ-BSA signals evaluated in 3×30 cells for values in I and 3×30 cells for values in J. Values are given as mean ± SEM. For specific values, see Table S1. One-way ANOVA; *, $P < 0.05$; **, $P < 0.01$. **(K)** SNX3 regulates intracellular survival of borreliae. Statistical evaluation of intracellular survival of borreliae in macrophages treated with SNX3-specific siRNA or control siRNA. Graphs show growth curves of borreliae recultured from respective macrophage cell lysates. Number of recultured borreliae in growth medium (10^4/ml) is indicated on the y axis, and days after start of the experiment are indicated on the x axis. $n = 3$, two-tailed Student's t test; *, $P < 0.05$.

recultured from macrophage lysates from both control and SNX3-depleted cells. However, spirochete numbers in cultures from SNX3-depleted cells were higher than those from control cells and exceeded control values significantly by a factor of 2.3 at day 10 of reculture (Fig. 2 K), suggesting enhanced viability of borreliae within macrophages as a result of SNX3 depletion.

SNX3 and phosphoinositols colocalize at borreliae phagosomes

SNX3 is one of the smallest SNX isoforms, mainly consisting of a PX domain that binds phosphatidylinositols (Cozier et al., 2002; Mizutani et al., 2009). To investigate the molecular mode of action of SNX3 at borreliae phagosomes, we thus first assessed enrichment and potential colocalization of phosphoinositols with SNX3 at these structures. Macrophages were transfected with labeled reporter constructs for phosphoinositols and RFP-SNX3, incubated with borreliae, and analyzed by confocal microscopy. Reporter constructs included PX-p40phox-GFP for PI(3)P (Kanai et al., 2001), TAPP1-PH-GFP for PI(3,4)P_2 (Kimber et al., 2002), GFP-ML1Nx2 for PI(3,5)P_2 (Hammond et al., 2015), PH-Akt-GFP for phosphatidylinositol (3,4,5)-trisphosphate (PI(3,4,5)P_3; Sason et al., 2009), P4M-SidM-GFP for PI(4)P (Hammond et al., 2014), PH-PLCδ1-GFP for PI(4,5)P_2 (Várnai and Balla, 1998), and GFP-PHD-Ing2 × 3 for PI(5)P (Gozani et al., 2003).

Klose et al.
SNX3 drives maturation of *Borrelia* phagosomes

Phosphoinositols that were enriched at borreliae phagosomes and colocalized with RFP-SNX3 included PI(3)P (Fig. 3, A–D), PI(3,4)P_2 (Fig. 3, E–H), PI(4)P (Fig. 3, I–L), and possibly PI(3,4,5)P_3 (Fig. S4, E–H), the latter due to the Akt-PH reporter construct binding to PI(3,4)P_2 and PI(3,4,5)P_3. Interestingly, enrichments of PI(3)P colocalizing with RFP-SNX3 were especially found at turning points of borreliae phagosomes, due to the helical shape of the spirochete, which is in line with reports of PI(3)P being enriched at sites of high membrane curvature (Rao et al., 2016; Daste et al., 2017). In contrast, no specific enrichment was detected for PI(3,5)P_2 (Fig. S4, A–D), PI(4,5)P_2 (Fig. S4, I–L), and PI(5)P (Fig. S4, M–P). To test whether SNX3 and the identified phosphoinositols could interact, GST fusions of WT SNX3 and of a mutant deficient in phosphoinositide binding (SNX3-Y71A; Xu et al., 2001) were bacterially expressed, purified, and incubated on phosphoinositide-spotted membranes with GST as a negative control. Development with either anti-SNX3 or anti-GST antibodies showed a strong signal for PI(3)P, but not for other phosphoinositides, including PI(3,4)P_2 and PI(4)P (Fig. 3, M and N). Strikingly, no respective signal was detectable in the case of the SNX3-Y71A mutant (Fig. 3, M and N).

To determine the source of PI(3)P at borreliae phagosomes, live-cell imaging was performed using macrophages expressing the PI(3)P sensor p40phox-GFP, either alone (Fig. S5 A and Video 5) or in combination with endosomal marker RFP-Rab5a (Fig. S5 B and Video 6). Interestingly, we observed a gradual accumulation of PI(3)P at borreliae phagosomes, with only occasional contact by PI(3)P- and Rab5a-positive endosomes. Taken together, these observations point to the local generation of PI(3)P at phagosomes, with endosomal delivery of PI(3)P probably only as a contributing source.

Phosphoinositide 3-kinase (PI3K) activity and binding of PI(3)P by SNX3 are required for borreliae compaction

The data so far indicated that SNX3 binds specifically to PI(3)P in vitro and colocalizes with this lipid prominently at borreliae phagosomes. Therefore, we next investigated whether presence of PI(3)P and its binding by SNX3 influence phagosomal compaction of borreliae. PI3K activity was inhibited in macrophages by the addition of Wortmannin and the presence of PI(3)P, using the reporter p40phox-GFP, and the addition of GFP-SNX3 at phagosomes was investigated in cells incubated with borreliae. Macrophages treated with DMSO as control showed regular enrichment of PI(3)P (Fig. 3 O) and GFP-SNX3 (Fig. 3 R) at borreliae phagosomes and also regular rates of borreliae compaction (49.9% ± 9.3%; Fig. 3 Q). Importantly, treatment with Wortmannin (1 µM) led to a loss of both PI(3)P (Fig. 3 P) and GFP-SNX3 (Fig. 3, S and T) enrichment at borreliae phagosomes and a decrease of borreliae compaction (21.6% ± 2.15%), corresponding to a 57% reduction, similar to values gained with SNX3 depletion by siRNA (Fig. 2 B).

To investigate the potential impact of PI(3)P binding by SNX3, siRNA-insensitive constructs of GFP-SNX3 and the GFP-SNX3-Y71A mutant deficient in PI(3)P binding were created. siRNA-insensitive constructs or GFP alone was expressed in macrophages treated either with SNX3 siRNA for depletion of endogenous SNX3 or with control siRNA. Cells

were incubated with borreliae, and phagosomal compaction was analyzed by confocal microscopy. Strikingly, the SNX3-Y71A mutant construct did not localize to borreliae phagosomes (Fig. 4, A–C). Also, expression of GFP-SNX3 WT and the Y71A mutant did not lead to significantly reduced rates of borreliae compaction in cells treated with control siRNA (60.1% ± 4.8% for GFP-SNX3 and 47.7% ± 7.4% for GFP-SNX3-Y71A vs. 71.3% ± 4.8% for GFP alone; Fig. 4 D). As expected, treatment with SNX3 siRNA led to an ~50% reduction of borreliae compaction in GFP-expressing controls (34.7% ± 6.4%). This was rescued to 94% of regular levels through expression of the siRNA-insensitive GFP-SNX3 WT construct (64.6% ± 2.8% compaction). However, expression of the GFP-SNX3-Y71A mutant was not able to rescue compaction, leading to 56% of regular levels of compaction (31.7% ± 3.4% compaction) and thus to values comparable to the GFP control (Fig. 4 D). Collectively, these results indicate that generation of PI(3)P by PI3K and binding of the lipid by SNX3 at the phagosomal coat are important for compaction of borreliae.

The C-terminal region of SNX3 is crucial for borreliae compaction

To systematically explore the impact of the different regions of SNX3 in localization to and compaction of borreliae phagosomes, the following GFP-fused constructs were created and tested for their localization at borreliae phagosomes: a construct missing the N-terminal region (SNX3-ΔN), a construct missing the N-terminal region and the subsequent α-helix (SNX3-PX+C), a construct missing the C-terminal region (SNX3-ΔC), a construct consisting of the N-terminal region and α-helix (SNX3-N+α), and a construct consisting of the C-terminal region (SNX3-C; Fig. 5 A). Compared with full-length GFP-SNX3, both SNX3-ΔN and SNX3-PX+C showed ~30% reduction in localization, while constructs missing the PX domain, SNX3-N+α and SNX3-C, failed to localize to phagosomes (Fig. 5 B). These data indicated a moderate but significant influence of the N-terminal region of SNX3 to phagosomal localization and also the absolute requirement of the PX region for this function. Surprisingly, the construct deleted only in the C-terminal region, consisting of 11 amino acid residues (Fig. 5 A), showed a >80% reduction in phagosomal localization (Fig. 5 B), indicating a crucial influence of this region. Collectively, these data indicated that localization of SNX3 to borreliae phagosomes involves multiple regions of SNX3, with the PX domain and the C-terminal region exerting the strongest influence.

To assess the influence of the different SNX3 regions on phagosome compaction, siRNA-insensitive constructs were created (for GFP-SNX3-ΔN, GFP-SNX3-PX+C, and GFP-SNX3-ΔC, as GFP-SNX3-N+α and GFP-SNX3-C are not targeted by the siRNA used) and overexpressed in macrophages that were treated with control or SNX3-specific siRNA (Fig. 5, C–R1), and compaction of borreliae in phagosomes was evaluated (Fig. 5 S1). As in previous experiments (Fig. 2 B), knockdown of SNX3 led to an ~50% reduction in phagosomal compaction, which could be fully rescued by overexpression of siRNA-insensitive full-length SNX3 and also by expression of either SNX3-ΔN or SNX3-PX+C. In contrast, expression of
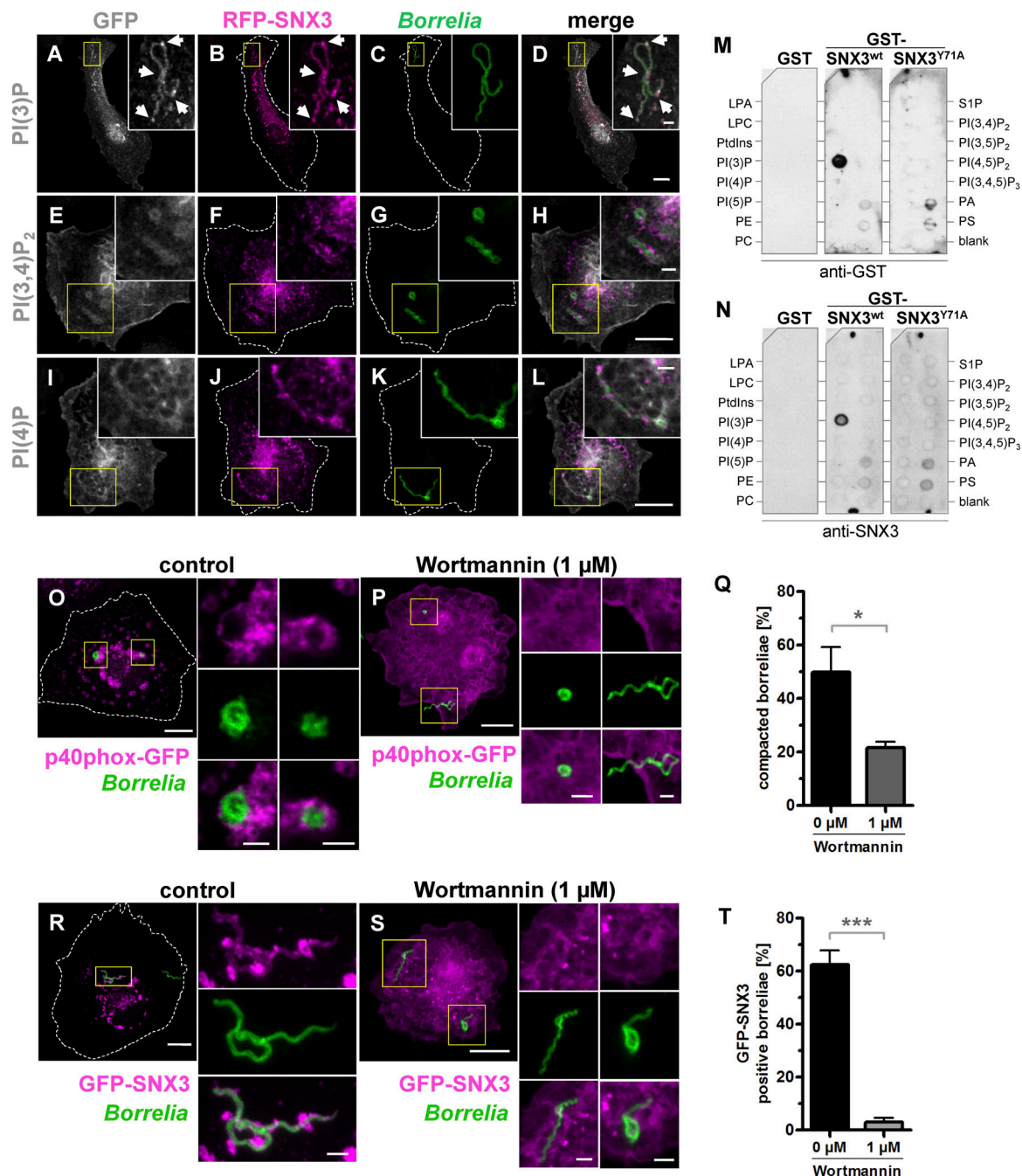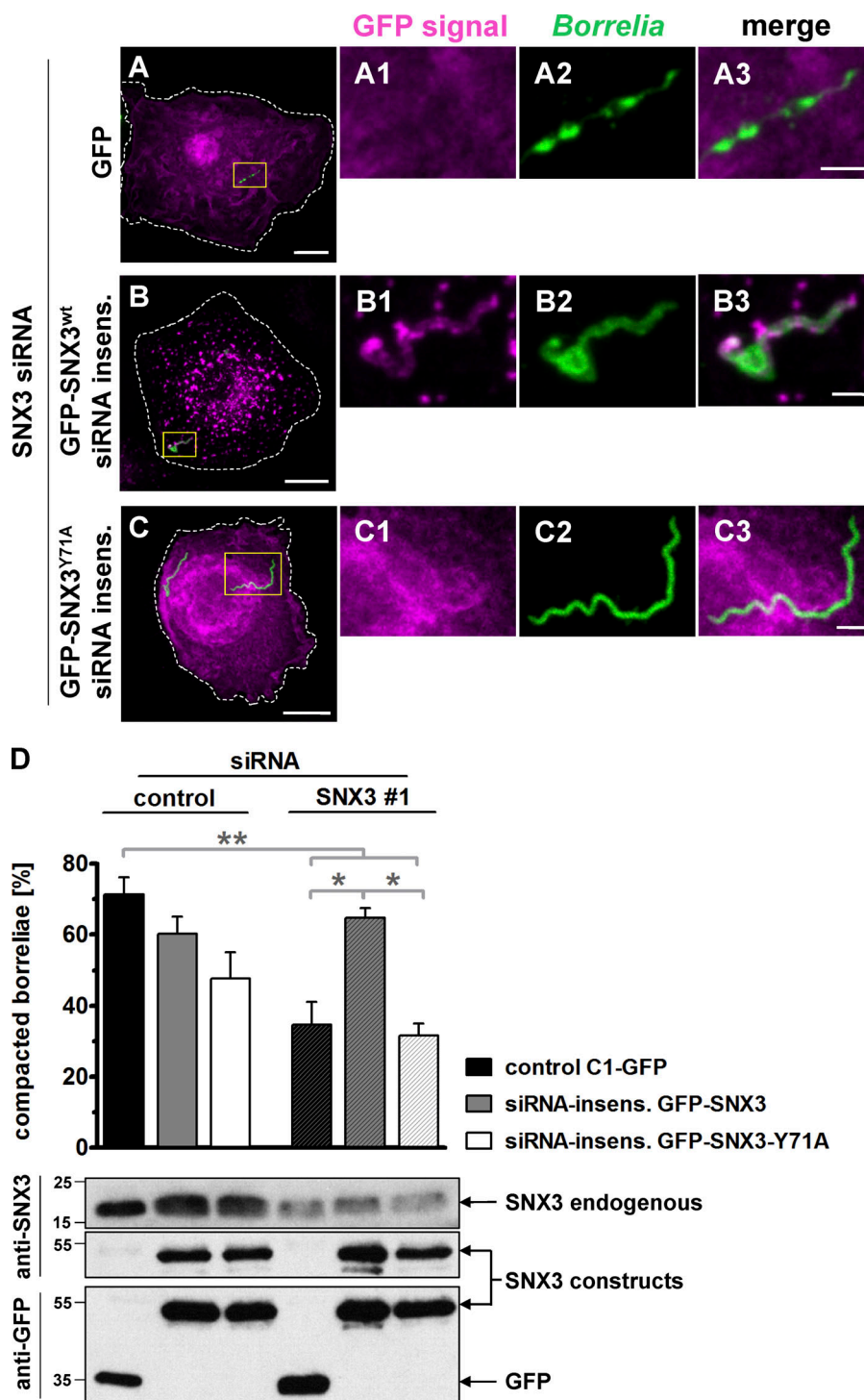
Figure 3. SNX3 binds to PI(3)P and colocalizes with PI(3)P at *B. burgdorferi*–containing phagosomes. (A–L) Confocal micrographs of macrophages coexpressing fluorescent probes for PI(3)P (A), PI(3,4)P_2 (E), or PI(4)P (I), and coexpressing RFP-SNX3 (B, F, and J), with internalized borreliae stained by antibodies (C, G, and K). Yellow boxes indicate areas shown enlarged as insets. Arrows indicate enrichments of PI(3)P and RFP-SNX3. Scale bars: 10 µm, and 1 µm for insets. **(M and N)** Binding of GST-fused SNX3 WT and SNX3-Y71A mutant on phosphatidylinositol-spotted strips incubated with GST alone or GST-SNX3 WT or GST-SNX3-Y71A mutant and developed with anti-GST antibody (M) or anti-SNX3 antibody (N). LPA, lysophosphatidic acid; LPC, lysophosphocholine; PA, phosphatidic acid; PC, phosphatidylcholine; PE, phosphatidylethanolamine; PS, phosphatidylserine; S1P, sphingosine 1-phosphate. **(O–T)** PI3K activity regulates compaction of borreliae. **(O, P, R, and S)** Confocal micrographs of macrophages expressing PI(3)P sensor p40phox-GFP (O and P) or GFP-SNX3 (R and S), with internalized borreliae stained by antibodies, with merges. Cells were treated with DMSO (0.1%) as control (O and R) or with PI3K inhibitor Wortmannin (1 µM; P and S); yellow boxes indicate areas shown enlarged as insets. Scale bars: 10 µm, and 1 µm for insets. **(Q and T)** Statistical evaluation of borreliae compaction in cells expressing p40phox-GFP (Q) or of GFP-SNX3 localization to borreliae phagosomes (T); cells were treated with Wortmannin or DMSO as control. $n = 3$ (3×30 cells). For specific values, see Table S1. Two-tailed Student's t test; *, $P < 0.05$; ***, $P < 0.001$. Error bars: mean ± SEM.

constructs lacking the PX domain, SNX3-N+α and SNX3-C, was accompanied by a strong reduction in phagosomal compaction comparable to levels of expression of GFP alone.

Moreover, expression of the construct lacking the C-terminal region, SNX3-ΔC, showed a similar inability to rescue phagosomal compaction (Fig. 5 S1). Interestingly, expression of

Figure 4. **PI(3)P binding by SNX3 regulates compaction of borreliae. (A–C)** Confocal micrographs of macrophages treated with SNX3-specific siRNA#1 and expressing GFP as control (A) or siRNA-insensitive constructs GFP-SNX3 (B) or GFP-SNX3-Y71A (C). Boxes in A–C indicate areas of detail images. GFP signals (magenta; A1, B1, and C1), with internalized borreliae stained by *B. burgdorferi*–specific antibody (green; A2, B2, and C2), and merges (A3, B3, and C3). Scale bars: 10 µm, and 2 µm in detail images. **(D)** Top: Statistical evaluation of borreliae compaction in cells treated with SNX3-specific siRNA and expressing indicated constructs. $n = 3$ (3×30 cells). For specific values, see Table S1. One-way ANOVA; *, $P < 0.05$; **, $P < 0.01$. Error bars: mean ± SEM. Bottom: Western blots of respective macrophage lysates, developed with SNX3-specific or GFP-specific antibody. The position of respective bands is indicated by arrows on the right, and molecular weight is indicated in kilodaltons on the left. Insens., insensitive.
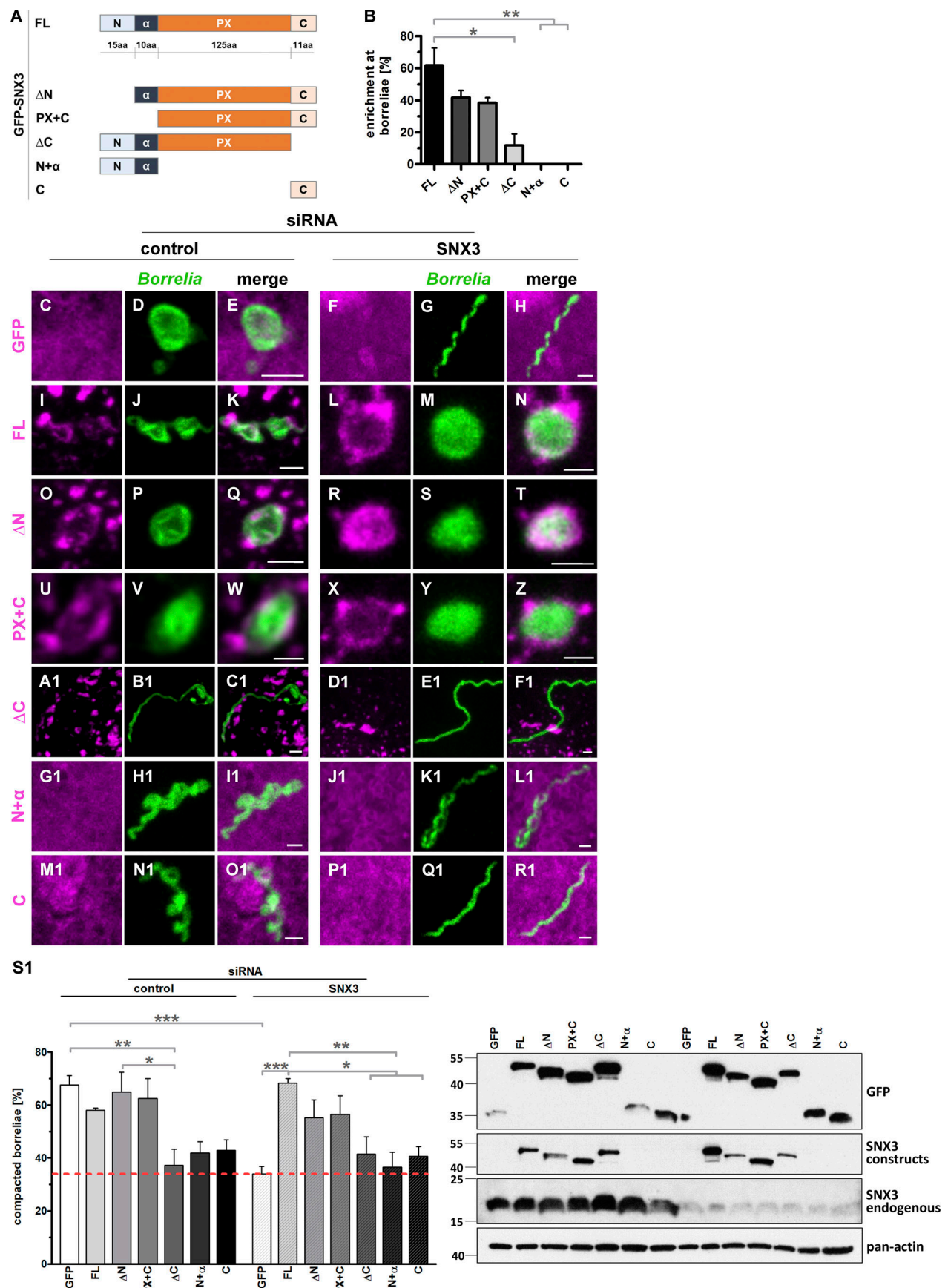
SNX3-ΔC, SNX3-N+α, or SNX3-C in control cells (i.e., with endogenous SNX3 still present) led to a similar reduction in phagosomal compaction (Fig. 5 S1), pointing to a respective inhibitory influence of these constructs. Collectively, these experiments showed that both the PX domain and the C-terminal region are required for regular phagosomal compaction of borreliae and that their impact on this process closely mirrors their ability to localize to borreliae phagosomes (Fig. 5, C–R1) and disturb this process in the presence of endogenous SNX3 (Fig. 5 B).

Galectin-9 is a SNX3 binding partner that drives borreliae compaction

We hypothesized that the impact of the SNX3 C-terminal region could be based on binding to an unknown interaction partner. To address this question, GFP-SNX3-C was expressed in macrophages, anti-GFP immunoprecipitation was performed, and the resulting precipitate was analyzed by mass spectrometry. Resulting hits were graded according to respective coverage and presence of unique peptides. Candidates included cytoskeletal proteins such as CKAP4 and MyoIe and vesicle-associated

Klose et al.
SNX3 drives maturation of *Borrelia* phagosomes

Figure 5. **The C-terminal region of SNX3 is crucial for localization to phagosomes and borreliae compaction. (A)** Graphic representation of SNX3 regions used in respective GFP-fused constructs: the N-terminal region (N), followed by an α-helical region (α), a PX domain, and a C-terminal region (C). **(B)** Enrichment of SNX3 constructs at borreliae phagosomes, with total number of phagosomes set to 100%. Values are presented as mean ± SEM, with 3 × 30 phagosomes analyzed. One-way ANOVA; *, P < 0.05; **, P < 0.01. For specific values, see Table S1. **(C–R1)** Colocalization of GFP-fused SNX3 constructs at borreliae phagosomes. Confocal micrographs of macrophages transfected with respective constructs (magenta), with borreliae stained by *B. burgdorferi*–specific antibody (green), and merges. Cells were treated with control siRNA or SNX3-specific siRNA, as indicated. Scale bars: 1 µm. **(S1)** Evaluation of borreliae phagosome compaction in macrophages expressing siRNA-insensitive SNX3 constructs. Top: Statistical evaluation of borreliae compaction in cells treated with control siRNA or SNX3-specific siRNA and expressing indicated constructs. $n = 4$ (4 × 30 cells). Dotted red line indicates level of borreliae compaction in SNX3-depleted control (GFP-expressing) cells. For specific values, see Table S1. One-way ANOVA; *, P < 0.05; **, P < 0.01; ***, P < 0.001. Bottom: Western blots of respective macrophage lysates, developed with GFP-specific or SNX3-specific antibody, the latter used for detection of both GFP-fused and endogenous forms of SNX3, with pan-actin as loading control. Molecular weight is indicated in kilodaltons on the left.

proteins such as SNX12, galectin-9, and Rab35 and the kinesins KIF5A, KIF5B, and KIF5C (Fig. S6 A). Candidates were reevaluated by performing a second set of GFP-SNX3-C immunoprecipitations and probing of Western blots with respective antibodies. Strikingly, of all candidates tested, only galectin-9 was coprecipitated to a detectable degree with SNX3-C (Fig. 6 A).

To further investigate the potential involvement of candidates in borreliae phagosomal regulation, immunofluorescence experiments using specific antibodies or expression constructs were performed using borreliae-infected macrophages. From all tested candidates (Fig. S1, M–O; and Fig. S6, B–M), only galectin-9 was localized to borreliae phagosomes, where it partially colocalized with endogenous SNX3. In particular, galectin-9 was enriched at compacted phagosomes or parts of phagosomes seemingly undergoing compaction (Fig. 6, B–F). To visualize this process in more detail, a GFP-fused construct of galectin-9 (GFP-galectin-9) was created and analyzed in confocal live cell imaging in RFP-SNX3 expressing cells. GFP-galectin-9 was found to be present at a motile vesicle population that was mostly distinct from the one positive for RFP-SNX3. Of note, galectin-9 was progressively enriched at SNX3-positive borreliae phagosomes, especially at sites of high curvature, and particular during later stages of compaction (Fig. 6 G and Video 4), correlating with the data gained earlier for endogenous galectin-9.
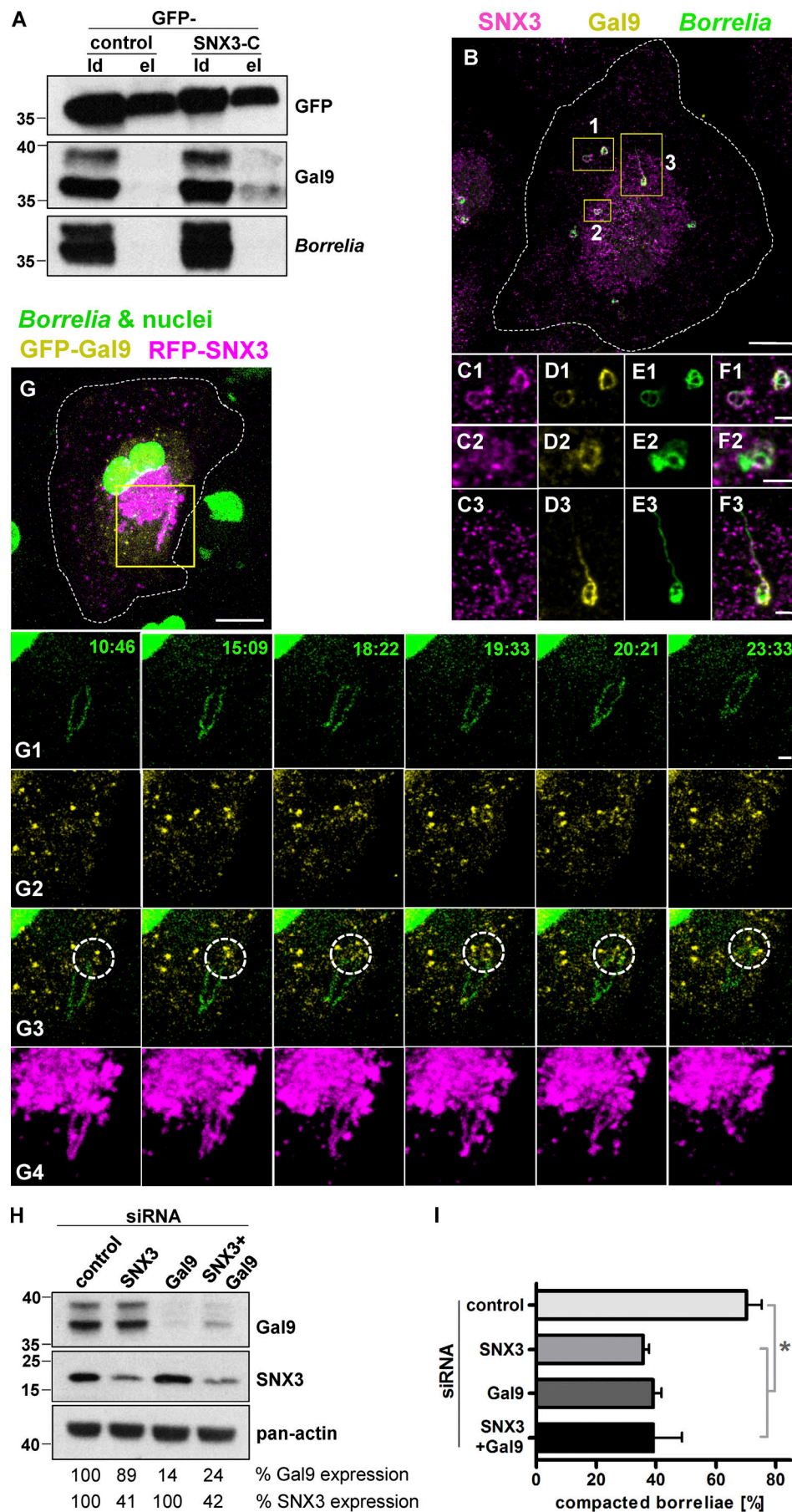
The data so far indicated that SNX3 recruits galectin-9 from a vesicular pool to the surface of borreliae phagosomes. To test the potential functional relevance of galectin-9 on borreliae phagosome compaction, galectin-9 knockdown was established by using two individual siRNAs, leading to a total reduction of 57% and 55%, respectively, of the two isoforms of galectin detected in Western blots. Importantly, depletion of galectin-9 did not impact on the expression levels of SNX3 and vice versa (Fig. 6 H). Macrophages were depleted for SNX3, galectin-9 or a combination of both, infected with borreliae, and analyzed by fluorescence microscopy for compaction of borreliae phagosomes. As shown before (Figs. 2 B, 4 D, and 5 S1), depletion of SNX3 led to an ~50% reduction in phagosomal compaction. Strikingly, depletion of galectin-9 led to a similar reduction. Moreover, combined depletion of SNX3 and galectin-9 also led to a reduction of ~50%, indicating, in the absence of an additive effect, that both proteins function in the same pathway (Fig. 6 I).

To investigate the potential impact of galectin-9 on phagosome maturation, macrophages transfected with control siRNA or galectin-9–specific siRNA were coincubated with GFP-expressing

borreliae and DQ-BSA and analyzed by confocal microscopy (Fig. 7, A–F). Fluorescence measurements showed that galectin-9 depletion by two siRNAs led to a reduction of DQ-BSA signals at *B. burgdorferi*–containing phagosomes of 18.1% and 20.1%, respectively, compared with controls (Fig. 7 G). Comparable to earlier results with SNX3 siRNA (Fig. 2 J), overall DQ-BSA–based fluorescence was unchanged (Fig. 7 H).

To further characterize the galectin-9 vesicle population and identify potential binding partners, anti-GFP immunoprecipitation of full-length galectin-9 was performed, and the resulting precipitate was analyzed by mass spectrometry. Resulting hits were graded according to respective coverage and presence of unique peptides. Promising candidates included RabGTPases such as Rab8a, Rab10, and Rab18; vesicle regulators of the flotillin family, flotillin-1 and -2; and the vesicle docking protein SNAP23 (Fig. S7 A). Respective GFP- or mCherry-labeled constructs were expressed in borreliae-infected cells, which were also stained for galectin-9. Further RabGTPases, including Rab4a, Rab6a, Rab7, Rab11, Rab14, Rab21a, Rab22a, Rab27a, and Rab43, were also included in this analysis to potentially identify the trafficking pathways of galectin-9 vesicles. From all tested candidates, enrichments of Rab6a, Rab8a, and Rab21 were found at borreliae phagosomes, which were, however, not localizing at galectin-9 vesicles (Fig. S7, B–Q). In contrast, flotillin-2 was found to prominently localize at galectin-9 vesicles, which could also be detected in live-cell imaging (Fig. 7 I).

Galectin-9 contains an N-terminal extension, as well as two carbohydrate-binding domains (CRDs), CRD1 and CRD2, which are connected by a linker region (Fig. 8 A). To determine the respective contribution of these domains to phagosomal compaction, respective siRNA-insensitive deletion constructs were generated (Fig. 8 A) and expressed in cells treated with control siRNA or galectin-9–specific siRNA (Fig. 8 B). Both an siRNA-insensitive WT construct and a construct missing the N-terminal extension (ΔN) were able to fully rescue compaction of borreliae phagosomes in galectin-9 siRNA–treated cells. By contrast, a construct missing the N-terminal extension and the CRD1 domain (linker+CRD2), as well as a construct missing the linker and the CRD2 domain (N+CRD1), showed compaction levels comparable to controls. A further construct missing the CRD2 domain (ΔCRD2) and a construct missing the CRD2 domain and the N-terminal extension (CRD1+linker) showed intermediate values that were not significantly different from controls. Of note, from all constructs tested, only the ΔN construct showed a fully vesicular localization comparable to the

Klose et al.
SNX3 drives maturation of *Borrelia* phagosomes

Journal of Cell Biology
https://doi.org/10.1083/jcb.201812106

3048

Figure 6. **Galectin-9 interacts with the SNX3 C-terminus and regulates borreliae compaction. (A)** Western blots of anti-GFP immunoprecipitations of lysates from macrophages expressing GFP as control or GFP-SNX3-C construct, developed with GFP-, galectin-9–, or *B. burgdorferi*–specific antibodies, with load (ld) and elution (el) fractions, as indicated. (Note that galectin-9 blot was reprobed for detection of borreliae. Comparison between respective lanes of SNX3-C elutions thus shows that the galectin-9 signal is not due to overspill of the load lane.) Molecular weight is indicated in kilodaltons. **(B–F)** Endogenous forms of SNX3 and galectin-9 localize to borreliae phagosomes. Confocal micrographs of macrophage stained for SNX3 and galectin-9, borreliae stained with *B. burgdorferi*–specific antibody. Yellow boxes indicate detail regions shown enlarged below, with merges (C1–F1, C2–F2, and C3–F3). **(G)** GFP-galectin-9 vesicles contact borreliae phagosomes. Shown are still images from live-cell video of macrophage expressing GFP-galectin-9 and RFP-SNX3, with borreliae and nucleus stained by Hoechst 33342 (Video 4). Yellow box indicates detail region shown enlarged in galleries (G1–G4) below. Time since start of experiment is indicated in minutes:seconds. Dotted circles indicate contact of galectin-9 vesicles with borreliae phagosomes. Scale bars: 10 µm for B and G, and 2 µm for insets. **(H)** Western blot of lysates from macrophages treated with control siRNA, SNX3-specific or galectin-9–specific siRNA, or a combination of both. Blots were developed with SNX3- or galectin-9–specific antibodies or with pan-actin antibody for loading controls. Molecular weight in kilodaltons is indicated on the left. **(I)** Evaluation of borreliae compaction in cells treated with control siRNA, SNX3 siRNA, or galectin-9 siRNA or a combination thereof. Values are given as mean ± SEM. Note the absence of additive effect in SNX3 and galectin-9 double knockdown. For specific values, see Table S1. *n* = 3. One-way ANOVA; *, P < 0.05.

WT. The N+CRD1 construct showed a mixture of dispersed and vesicular localization, while all other constructs showed dispersed localization (Fig. S7, R–V). The vesicular localization of galectin-9 constructs thus closely correlated with their respective ability to act in phagosomal compaction. Collectively, these results indicate that both CRDs are important for regular compaction levels of *B. burgdorferi* phagosomes, while the N-terminal extension, and possibly also the linker region, are not involved in this process.

We next tested whether the lectin activity of galectin-9 is involved in phagosome compaction. Interestingly, both CRDs differ in their affinities for specific carbohydrates. Accordingly, several critical amino acid residues have been identified that are necessary for binding of specific carbohydrates, including Ala46 for the binding of Forssman pentasaccharides (Nagae et al., 2008), Asn137 for poly-N-acetyllactosamine (Nagae et al., 2009), and Arg221 for sialylated oligosaccharides (Yoshida et al., 2010), the latter corresponding to Arg252 of the construct used in this study, due to a shorter linker region used in Yoshida et al. (2010). Respective siRNA-insensitive constructs were generated (Fig. 8 C) and tested for their ability to rescue regular phagosomal compaction levels. However, all of the mutants showed intermediate values for phagosome compaction rescue, which were also not significantly different from the negative control (Fig. 8 D). It is thus unlikely that binding of the specific carbohydrates mentioned above is a decisive factor for galectin-9–dependent regulation of phagosome compaction.

Collectively, these data show that galectin-9 is a novel binding partner of the SNX3 C-terminal region, is recruited to SNX3-positive borreliae phagosomes during later stages of compaction, and functions in the same pathway as SNX3 in phagosomal compaction and that both of its CRDs are important for this process.

SNX3 enables recruitment of Rab5a and galectin-9 to borreliae phagosomes

Collectively, the data indicated that SNX3 enables the contact of two distinct vesicle populations, carrying either Rab5a or galectin-9, with borreliae-containing phagosomes. We thus tested the importance of SNX3 in recruiting Rab5a and galectin-9 by measuring their respective enrichment at phagosomes using fluorescence microscopy in RFP-Rab5a–expressing cells stained for galectin-9 and treated with control siRNA or SNX3-
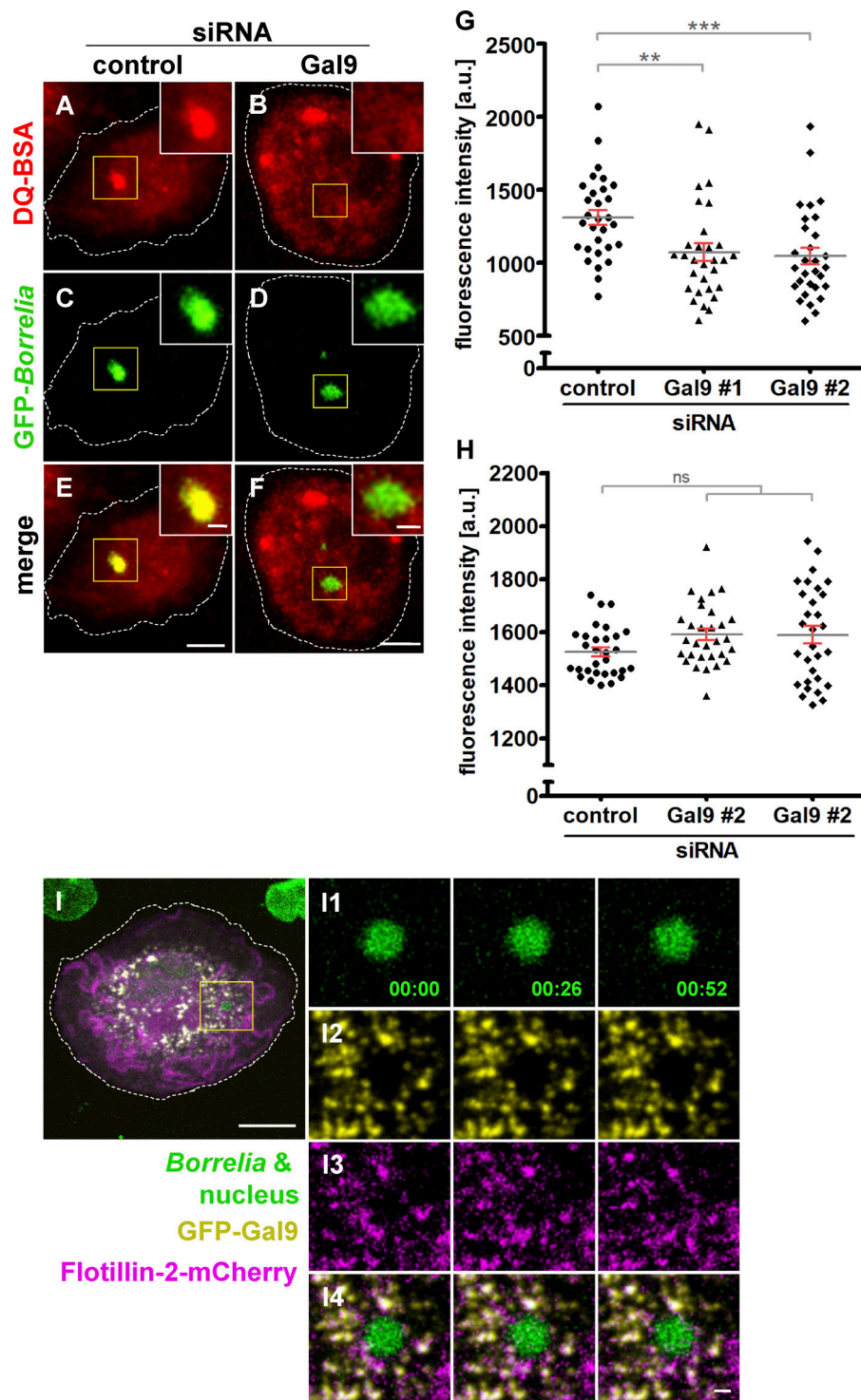
specific siRNA (Rab5a was overexpressed, as staining of endogenous Rab5a resulted in high background; Fig. 9, A and B). Signal intensities were measured by analyzing phagosome-surface–associated fluorescence in confocal stacks (300 nm distance in z) that encompassed complete phagosomes. Indeed, phagosome-associated fluorescence was strongly reduced in both cases, with RFP-Rab5a–based signals showing a 54% reduction (17,497 a.u. ± 2,468 a.u. for SNX3 siRNA–treated cells compared with 38,078 a.u. ± 5,603 a.u. for controls; Fig. 9 C) and galectin-9–based signals showing a 41% reduction (1,685 a.u. ± 144.5 a.u. for SNX3 siRNA treated cells, compared with 2,837 a.u. ± 291.2 a.u. for controls; Fig. 9 D). Importantly, the respective analyzed volumes around borreliae phagosomes were not significantly different (Fig. 9 E). These results show that SNX3 is required for the recruitment of regular levels of both Rab5a and galectin-9 to the surface of borreliae-containing phagosomes.

Discussion

In this study, we identify SNX3 as a regulator of compaction and maturation of borreliae-containing phagosomes in primary human macrophages. SNX3 is present at Rab5a-positive vesicles that contact the phagosomal coat, becomes progressively enriched at phagosomes, and is lost from phagosomes only upon their full compaction. In turn, siRNA-mediated depletion of SNX3 leads to strongly reduced compaction of borreliae phagosomes, a reduction in their proteolytic activity, and increased intracellular survival of borreliae, pointing to an important role of SNX3 in the intracellular processing of spirochetes by human immune cells. SNX3 thus provides a crucial link between endosomes and phagosomes, as recruitment of endosomal Rab5a to borreliae phagosomes is essential for the initiation of phagosomal compaction and phagolysosomal maturation (Naj and Linder, 2015).

A major functional feature of SNXs is the binding of phosphoinositides, including PI(3)P and PI(3,5)P_2, through their PX domains (Cozier et al., 2002). Earlier, through use of microtiter plates, the PX domain of SNX3 has been shown to interact mostly with PI(3)P and to a lesser degree with PI(3,5)P_2 (Xu et al., 2001). Using phosphoinositide-spotted strips, we could confirm the preferential binding of the SNX3 PX domain to PI(3)P. This is a strong indication that from the three phosphoinositides that are enriched at borreliae phagosomes, (PI(3)P, PI(3,4)P_2, and PI(4)P),

Figure 7. **Galectin-9 regulates maturation of B. burgdorferi–containing phagosomes. (A–F)** Confocal micrographs of macrophages incubated with DQ-BSA (A and B), to visualize proteolysis, with internalized GFP-expressing borreliae (C and D), with merges (E and F). Macrophages were treated with control siRNA (A, C, and E) or galectin-9–specific siRNA (B, D, and F). Scale bars: 10 µm for overview images and 1 µm for insets. **(G and H)** Evaluation of DQ-BSA–based fluorescence intensities at macrophage phagosomes containing borreliae (G) or overall cellular DQ-BSA fluorescence (H) Fluorescence intensities are indicated on the y axis. Macrophages were treated with control siRNA or two individual galectin-9–specific siRNAs, as indicated. $n = 3$, with DQ-BSA signals evaluated in 3×30 cells. Values are given as mean ± SEM. For specific values, see Table S1. One-way ANOVA; **, $P < 0.01$; ***, $P < 0.001$. **(I)** Galectin-9 dynamically colocalizes with flotillin-2 at vesicles. Still images from confocal time lapse of macrophage with an internalized *B. burgdorferi* cell, with the spirochete and nucleus stained by Hoechst 33342 (I1); GFP-galectin-9 shown in yellow (I2), and flotillin-2-mCherry is shown in magenta (I3), with merge (I4). Time since start of experiment is indicated in minutes:seconds. Scale bars: 10 µm, and 1 µm for insets.
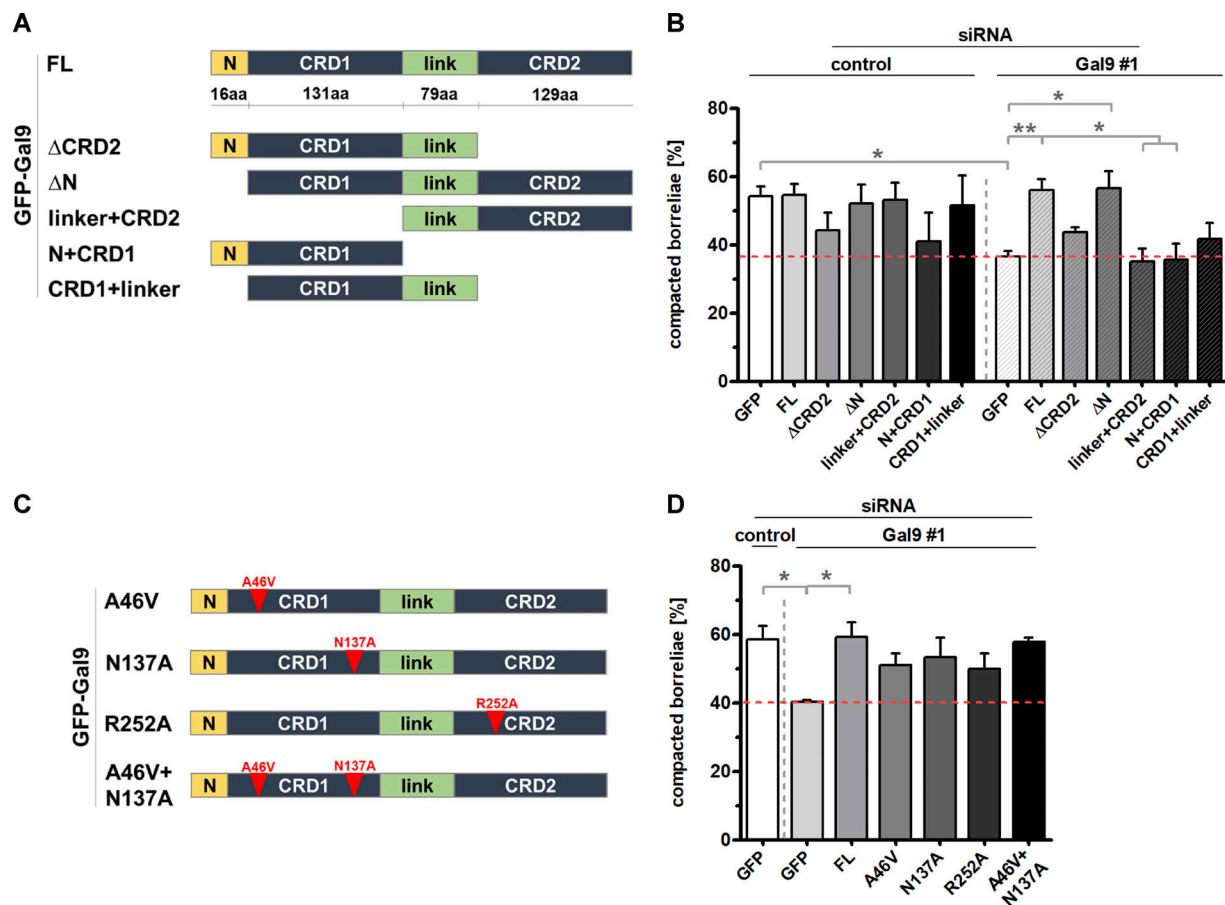
SNX3 binds only PI(3)P in cells. This is further corroborated by experiments using the PI3K inhibitor Wortmannin, which resulted in a dispersed localization of the PI(3)P reporter construct. Coincidentally, SNX3 was no longer detectable at phagosomes, and levels of borreliae phagosomal compaction were strongly reduced, similar to those measured under siRNA-induced depletion of SNX3. Moreover, an siRNA-insensitive SNX3 mutant defective in PI(3)P binding (Xu et al., 2001) failed to localize to borreliae phagosomes and could not rescue borreliae compaction

upon depletion of endogenous SNX3. In conclusion, we find that the presence of both SNX3 and PI(3)P is required for regular processing of borreliae and that SNX3 cannot be recruited to phagosomes if its phosphoinositide binding partner is absent from the phagosomal coat.

Use of the PI3K inhibitor Wortmannin, leading to a dispersed localization of the PI(3)P sensor, indicates that PI(3)P at phagosomes and endosomes is likely generated by phosphorylation of inosities and not by dephosphorylation of phosphoinositides

Figure 8. **Evaluation of borreliae phagosome compaction in macrophages expressing siRNA-insensitive galectin-9 constructs. (A and C)** Domain structure of galectin-9, showing an N-terminal extension (N) and two CRDs (CRD1 and CRD2), which are connected by a linker region (link), and respective deletion constructs (A) or point mutants defective in the binding of specific carbohydrates (see text; C). **(B and D)** Statistical evaluation of borreliae compaction in cells treated with control siRNA or galectin-9–specific siRNA and expressing indicated deletion (B) or point mutation (D) constructs. B: at least $n = 4$ (4 × 20 cells); D: $n = 3$ (3 × 15 cells). Dotted red line indicates level of borreliae compaction in galectin-9–depleted control (GFP-expressing) cells. For specific values, see Table S1. One-way ANOVA; *, $P < 0.05$; **, $P < 0.01$. Error bars: mean ± SEM.

such as $PI(3,4)P_2$. Moreover, as live-cell imaging revealed a gradual enrichment of $PI(3)P$ at borreliae phagosomes, with only occasional contact by $PI(3)P$- and Rab5a-positive endosomes, this points to the local generation of the phospholipid as a major source of phagosomal $PI(3)P$, with endosomal delivery probably only as a contributing source.

Formation of $PI(3)P$ by recruiting and activating class III PI3K is generally attributed to Rab5 activity. While we cannot entirely rule out such a mechanism, our data point to Rab5a recruitment from endosomes being downstream of $PI(3)P$ generation at borreliae phagosomes. Along similar lines, Rab5a is generally also placed upstream of Rab22a, which is reversed for borreliae phagosome compaction (Naj and Linder, 2015). It is thus possible that the molecular key players for phagosome development are retained in either scenario, while their functional interrelationship can apparently be changed.

Phosphatidylinositol 3-phosphates are present at sites of high membrane curvature (Marat and Haucke, 2016), because PI3K is preferentially active at these sites (Hübner et al., 1998). Indeed, we could observe local enrichments of both $PI(3)P$ and SNX3 at curved sites of borreliae phagosomes. It is thus likely that these

$PI(3)P$ enrichments serve as preferential docking sites for SNX3 vesicles to borreliae phagosomes. This would also tie in with earlier observations of Rab5a vesicles contacting borreliae phagosomes preferentially at curved sites (Naj and Linder, 2015). It is thus tempting to speculate that the helical spirochete morphology and the resulting phagosomal shape could actually drive phagosomal maturation by providing multiple sites of positive local curvature, thus leading to enrichment of $PI(3)P$, resulting in the docking of SNX3/Rab5a vesicles. Moreover, it would help to explain the fact that SNX3 stays enriched at borreliae phagosomes until compaction is completed, as only fully globular phagosomes would not provide local discontinuities in membrane curvature.

Phosphoinositide binding through the PX domain and curvature sensing by a BAR domain enable SNXs to function as coincidence detectors of membrane curvature subdomains (Carlton et al., 2005). However, SNX3 is one of the smallest SNX family members and does not contain a BAR domain. The only BAR domain–containing SNX detected at borreliae phagosomes is SNX1, and siRNA-mediated depletion of SNX1 did not influence compaction of borreliae. This does not, of course, rule out
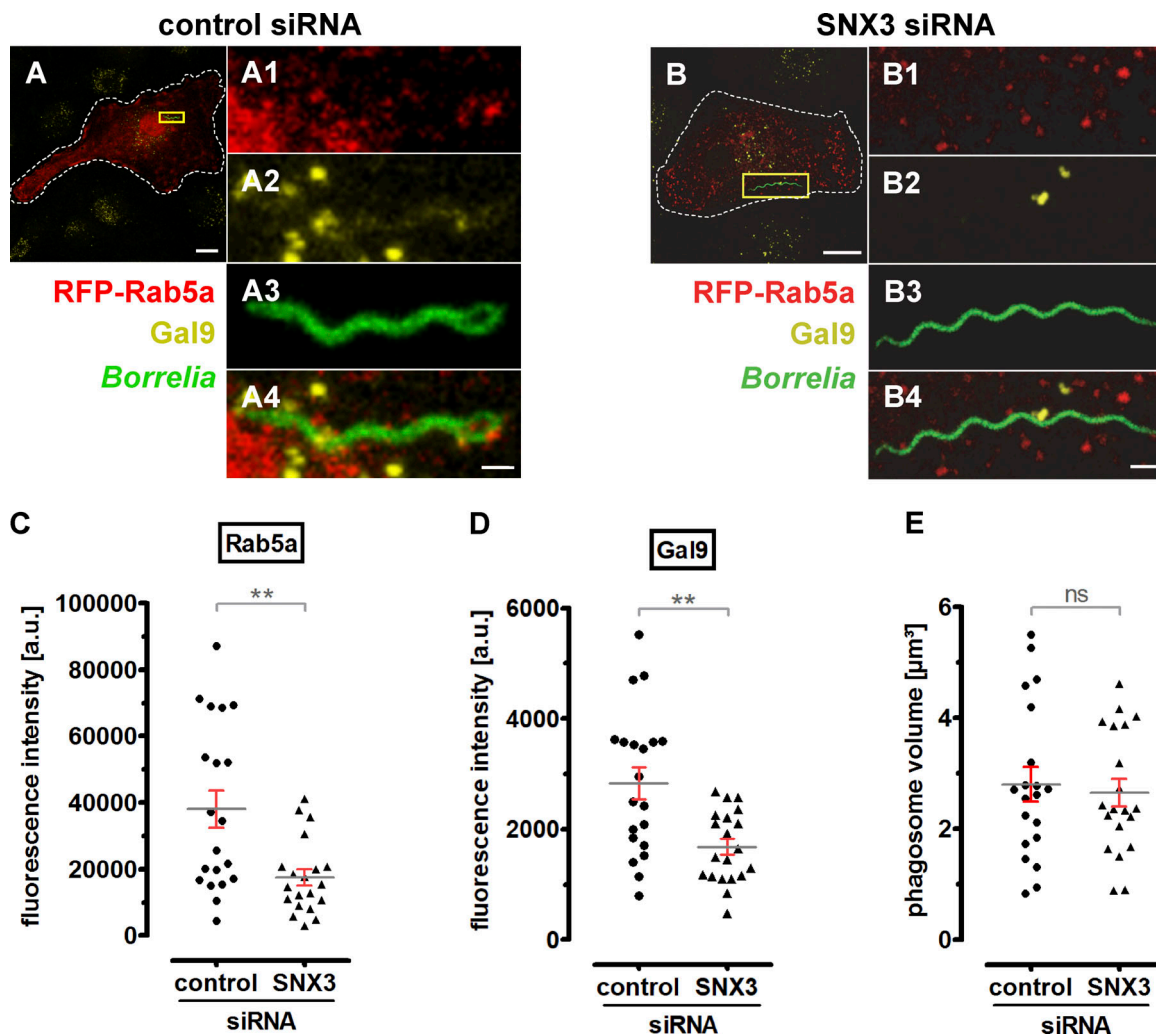
control siRNA **SNX3 siRNA**

A / A1 / A2 / A3 / A4
RFP-Rab5a / Gal9 / *Borrelia*

B / B1 / B2 / B3 / B4
RFP-Rab5a / Gal9 / *Borrelia*

C Rab5a D Gal9 E

Figure 9. **SNX3 enables recruitment of Rab5a and galectin-9 to borreliae phagosomes. (A and B)** Confocal micrographs of macrophages expressing RFP-Rab5 and stained for galectin-9 using specific antibody, incubated with GFP-expressing borreliae, and treated with control siRNA (A) or SNX3-specific siRNA (B). Scale bars: 10 µm for overview images and 1 µm for detail images. **(C–E)** Statistical evaluation of RFP-Rab5a– (C) and galectin-9–based (D) fluorescence intensities at borreliae phagosomes in cells treated with control siRNA or SNX3-specific siRNA, with respective measured volume of confocal stacks in cubic micrometers. Values are given as mean ± SEM ($n = 3 × 20$). For specific values, see Table S1. Two-tailed Student's t test; **, $P < 0.01$.

that another SNX among those not tested in the initial analysis could play a role in borreliae compaction and processing.

Of note, SNX3 does not form heterocomplexes with other SNXs (Haft et al., 1998), and it has been speculated that SNX3 binding of PI(3)P could prevent the binding of other SNXs to membranes (Worby and Dixon, 2002). However, the clear effect of SNX3 depletion on borreliae compaction, with its binding partner PI(3)P still being localized to phagosomes, seems to argue for a specific role of SNX3 in the processing of borreliae, which cannot be substituted by another SNX. It is also worth mentioning that the PX domain of SNXs is not highly conserved in terms of amino acid sequence, but as a structural fold (Teasdale et al., 2001; Worby and Dixon, 2002). It is thus possible that the PX domain of SNX3 is able to interact with further surface elements of the phagosomal coat, thus ensuring a specific requirement for SNX3 in borreliae compaction. Moreover, considering the presence specifically of SNX3 at Rab5a-positive vesicles and the comparable impact of SNX3 or Rab5a depletion

(50–60% reduction) on borreliae compaction (Naj and Linder, 2015), this seems to point to SNX3 as the requisite SNX in Rab5a-regulated intracellular processing of spirochetes.

SNX3 largely consists of a central PX domain, with short flanking N- and C-terminal regions. Molecular dissection and generation of deletion constructs further showed, as expected, that the PX domain is absolutely required for localization to phagosomes and borreliae compaction, while the N-terminal region and its adjacent α-helical region had only limited impact. Of note, the SNX3 N-terminal region has been shown to bind retromer complex (Lucas et al., 2016), and the SNX3–retromer complex has recently been shown to recruit a membrane remodeling complex that is required for Wntless recycling at endosomes (McGough et al., 2018). A similar mechanism could thus, in principle, be involved in membrane recycling at borreliae phagosomes. However, a SNX3 deletion construct lacking the N-terminal region and the subsequent α-helical region showed only an approximately one-third reduction of

phagosomal localization, while a respective siRNA-insensitive rescue construct was able to restore phagosome compaction to approximately two thirds of control levels, although without statistically significant difference to controls. It is thus conceivable that a SNX3–retromer complex could play a role in membrane and protein recycling at borreliae phagosomes, but its overall influence on borreliae compaction and processing would most likely be limited. Of note, the SNX3–retromer complex functions independently of those retromer complexes that contain BAR domain SNXs (Lucas et al., 2016), and the latter could thus possibly play a role in intracellular processing of borreliae. Still, these results make a retromer-independent role of SNX3 in borreliae phagosome compaction more likely.

Accordingly, and in contrast to experiments regarding the N-terminus, we found that the short and previously uncharacterized C-terminal region of SNX3 is critically required for both localization and function of SNX3 at phagosomes. Respective immunoprecipitations and mass spectrometry analyses led to the identification of several potential binding partners of this region, including kinesins such as KIF5A, KIF5B, and KIF5C, cytoskeleton-associated proteins such as CKAP4 and Myo1e, and others. Strikingly, from all tested candidates, only galectin-9 could be immunoprecipitated from lysates of borreliae-infected cells, and only galectin-9 localized to borreliae phagosomes. Therefore, while we cannot rule out potential roles for these other candidate proteins, our initial analyses make a respective impact on SNX3-dependent processing of borreliae unlikely. Of note, only a small fraction of the total cellular pool of galectin-9 coprecipitated with the SNX3 C-terminus (Fig. 6 A), probably representing the fraction of galectin-9 that is binding SNX3 at borreliae phagosomes.

siRNA-mediated depletion further confirmed a role for galectin-9 in phagosomal compaction of borreliae. Moreover, combined depletion of SNX3 and galectin-9 did not lead to additive effects on borreliae compaction, indicating that both proteins function in the same pathway. Intriguingly, live-cell imaging showed that galectin-9 is present at a vesicle population that is clearly distinct from the one carrying SNX3 and Rab5a. Galectin-9 vesicles were mostly recruited at later stages of phagosome processing, with SNX3 already enriched at the phagosomal coat. It is thus very likely that galectin-9 functions downstream of SNX3 recruitment in phagosome maturation. Use of several deletion constructs showed that both CRDs are important for localization of galectin-9 to vesicles and for borreliae phagosome compaction. Further point mutants defective in binding to specific carbohydrates were not able to rescue regular compaction levels. However, we cannot rule out that galectin-9 functions by its lectin activity in this process, for example, through binding of other carbohydrates or of carbohydrate side chains of glycosylated proteins.

Galectins were initially discovered as binding partners of carbohydrates on the cell surface but have subsequently also been described as regulators of protein and membrane trafficking (Delacour et al., 2009; Johannes et al., 2018). Galectin-9 in particular has been shown to be involved in the response to lysosomal membrane damage by activating AMPK (Jia et al., 2018) and in limiting *Mycobacterium tuberculosis* infections in human macrophages through induction of IL-1β secretion (Sada-Ovalle et al., 2012). While the initiation of bactericidal pathways may play a role in galectin-9 regulation of borreliae processing, the impact of galectin-9 on phagosome compaction appears to be more related to the role of galectins in membrane trafficking pathways (Delacour et al., 2009). Of note, oligomerization of galectins has been associated with the generation of membrane curvature (Lakshminarayan et al., 2014; Johannes et al., 2016), and it should be highly interesting to unravel the exact role of galectin-9 in the curvature-sensitive process of borreliae phagosome compaction. Interestingly, another member of the galectin family, galectin-3, is recruited from a cytoplasmic pool to the inner leaflet of damaged phagosomes, thus functioning as a reporter of phagosome rupture (Paz et al., 2010; Ehsani et al., 2012). In contrast, we show here that galectin-9 is present at intracellular vesicles in macrophages and that it regulates the compaction of intact phagosomes, thus driving their maturation and borreliae degradation.

We further show that the majority of galectin-9 vesicles are also positive for flotillin-2, a member of the flotillin family implicated in the regulation of membrane and protein recycling pathways (Meister and Tikkanen, 2014). It is thus possible that galectin-9 exerts its role in borreliae phagosome compaction, at least in part, through the recruitment of flotillin-2. Flotillins have been shown to associate with the Rab11a- and SNX4-positive recycling compartment in HeLa cells to control E-cadherin trafficking (Solis et al., 2013). In MDA-MB-231 breast cancer cells, flotillins are associated with a Rab7-positive endosomal recycling compartment and regulate trafficking of the metalloproteinase MT1-MMP (Planchon et al., 2018). Interestingly, galectin-3 has been shown to be endocytosed by a flotillin-dependent pathway in MDCK cells (Straube et al., 2013). Taken together, these findings could point to a connection between members of the galectin and flotillin, but also of the Rab and SNX families, in the control of endosomal recycling pathways, with the individual family members involved potentially depending on the specific cellular context. An in-depth study of the exact role of flotillin in borreliae phagosome compaction and its interplay with galectin-9 and SNX3 should yield further important insights into this process. Moreover, the identification of flotillin-2 as an independent marker for galectin-9 vesicles should enable further galectin-9 knockdown and re-complementation experiments to unravel the mechanism that galectin-9 uses to regulate borreliae phagosomes compaction, such as vesicle–phagosome contact, membrane extrusion, or others.

Collectively, our data pointed to SNX3 being (i) a linker between Rab5-positive endosomes to sites of PI(3)P enrichment at the phagosomal coat and (ii) an adapter for the recruitment of galectin-9–positive vesicles to these sites. This was corroborated by experiments in SNX3 siRNA-treated cells, which showed strongly reduced levels of both Rab5a and galectin-9 at the phagosome surface. SNX3 thus appears to be crucial for the recruitment of both vesicle populations to *B. burgdorferi*–containing phagosomes, and it is possible that it also plays a respective role in other scenarios of infection or phagosomal processing.

Klose et al.
SNX3 drives maturation of *Borrelia* phagosomes

Journal of Cell Biology   3053
https://doi.org/10.1083/jcb.201812106

Importantly, SNX3 has been described to localize to phagosomes in human dendritic cells (Chua and Wong, 2013) and to SCVs in HeLa cells (Braun et al., 2010), the latter also involving PI(3)P, Rab5, and the generation of membrane tubules. However, there are important differences between these earlier models and the pathway that we describe here. The SCV is actively established by *Salmonella* within host cells and aims at the generation of a replication-enabling environment. The system of membrane tubules that is generated by SNX3 around the SCV thus supports survival of *Salmonella*. By contrast, the function of SNX3 in compaction of borreliae phagosomes leads to phagolysosome maturation and intracellular destruction of the spirochete. In consequence, depletion of SNX3 in *Salmonella*-infected cells led to reduced intracellular survival of *Salmonella* (Braun et al., 2010), while depletion of SNX3 in *B. burgdorferi*–infected macrophages leads to enhanced survival of spirochetes.

Moreover, several regulators common to SCV and borreliae phagosome maturation show a different subcellular localization and a different connectivity in terms of signaling pathways. Accordingly, Rab5 is present on the *Salmonella* phagosome and regulates the generation of PI(3)P, leading to recruitment of SNX3 (Braun et al., 2010). In contrast, Rab5a is not present at *B. burgdorferi* phagosomes, and vesicles that contain Rab5a, but also SNX3, can dock at *B. burgdorferi* phagosomes by SNX3 binding to PI(3)P on the phagosome coat. In addition, the subsequent recruitment of galectin-9, which apparently functions downstream of SNX3 in borreliae processing, has not been described so far for other systems of phagosome maturation. It should be highly interesting to uncover the underlying principles for the differential use of these molecular players in these scenarios of phagocytic processing that lead to such diverse outcomes of the infectious process. Bacterial effector proteins such as SopB (Braun et al., 2010) and the host cell type are likely to play a role.

Collectively, we identify SNX3 as a central hub for regulators of phagosomal compaction and intracellular processing of borreliae by primary human macrophages. SNX3 is present at Rab5a-positive endosomes, and its PX domain enables endosome–phagosome contact by binding to PI(3)P at the phagosomal coat. Moreover, besides providing a docking system for Rab5a-positive vesicles, SNX3 also recruits, by its C-terminal region, galectin-9, which we identify as a further regulator of phagosome compaction. SNX3 thus recruits two distinct vesicle populations to borreliae phagosomes whose molecular cargoes contribute to phagosome maturation and intracellular processing of borreliae by macrophages (Fig. 10). These results point to an important retromer-independent role of SNX3 in membrane recycling from phagosomes. It will be important to determine which individual steps of phagosome compaction and maturation are specifically affected by each of these players and elucidate the molecular mechanisms involved, especially in regard to the regulation of their spatiotemporal activity. Intriguingly, these data also suggest that the helical shape of *B. burgdorferi* itself, providing sites of high curvature and thus of local PI(3)P enrichment at phagosomes, may be one of the driving elements underlying efficient elimination of spirochetes by immune cells.

Materials and methods

Bacterial strains and growth conditions
A WT *B. burgdorferi* B31 ATCC 35210 strain and GFP-expressing *B. burgdorferi* GCB726 (provided by P. Kraiczy, University Hospital Frankfurt, Frankfurt, Germany) were cultivated as described before (Naj et al., 2013). TOP10 One Shot and DH5α *Escherichia coli* strains (Invitrogen) were used for transformation, cloning, and DNA plasmid amplification; L-arabinose–inducible *E. coli* BL21 was used for recombinant protein expression of GST constructs (Invitrogen).

Eukaryotic cell culture
Primary human monocytes were isolated from buffy coats (kindly provided by Frank Bentzien, Transfusion Medicine, UKE, Hamburg, Germany) by centrifugation in Ficoll; 12.5 ml blood was coated on 15 ml Ficoll (PromoCell) and centrifuged for 30 min at 4°C and 460 ×*g*. Leukocyte fractions were transferred in a new 50-ml Falcon tube and filled up to 50 ml with cold RPMI 1640 medium (Invitrogen). Cells were washed twice in RPMI 1640 and centrifuged for 10 min as described above. Enriched leukocytes were resuspended in 400 µl monocyte buffer (5 mM EDTA and 0.5% human serum albumin in Dulbecco's PBS [DPBS], pH 7.4), mixed with 100 µl of a suspension of magnetic beads coupled to CD14 antibodies (Miltenyi Biotec) and incubated for 15 min on ice. The mixture was then loaded on a MS+ Separation column (Miltenyi Biotec) previously placed in a magnetic holder and equilibrated with 500 µl cold monocyte buffer. Trapped CD14+ monocytes were washed on column with 500 µl monocyte buffer and after the removal of the magnet were eluted with 1 ml monocyte buffer into 15 ml cold RPMI 1640. After centrifugation for 10 min at 4°C and 460 ×*g*, the supernatant was removed and cells were resuspended in 40 ml RPMI 1640 and seeded on a 6-well plate (Sarstedt) at a density of 10^6 cells per well. After adhesion of monocytes, RPMI medium was replaced by 2 ml monocyte culture medium (RPMI 1640 substituted with 15% human serum [prepared in-house] and 100 µg/µl penicillin/streptavidin). Monocytes were cultivated in an incubator at 37°C, 5% CO_2, and 90% humidity; every 3–4 d, the culture medium was replaced by fresh medium. Cells were cultured in RPMI containing 20% autologous serum at 37°C, 5% CO_2, and 90% humidity.

Antibodies and constructs
For details on antibodies and constructs, please see Table S2.

Cloning of GFP-SNX3 deletion constructs
Full-length GFP-SNX3 was a kind gift of S. Grinstein (Hospital for Sick Children, Toronto, Canada). Based on this plasmid, five deletion constructs were generated by PCR and cloning into pEGFP vector using KpnI and BamHI restriction sites. The following primers were used: P01+P02 for GFP-SNX3-ΔC, P01+P03 for GFP-SNX3-N+α, P04+P05 for GFP-SNX3-ΔN, P06+P05 for GFP-SNX3-PX+C, and P07+P08 for GFP-SNX3-C. For details on PCR primers, see Table S2.

Generation of GFP-SNX3 PX mutant and siRNA-insensitive constructs
Generation of PX domain mutant GFP-SNX3 (Y71A) was done with QuikChange Site-Directed Mutagenesis PCR (Agilent) by
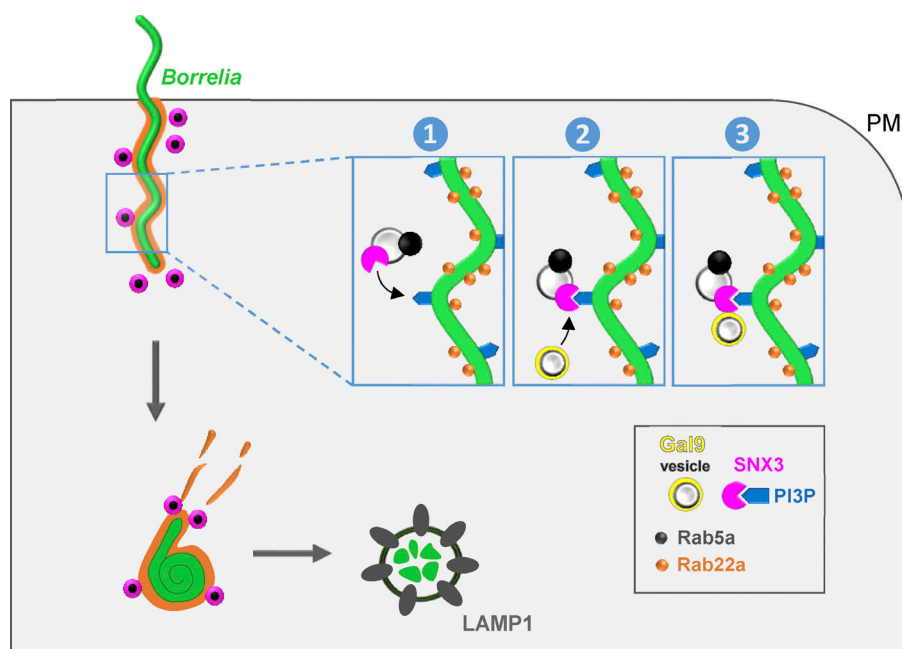
Klose et al.
SNX3 drives maturation of *Borrelia* phagosomes

Journal of Cell Biology 3054
https://doi.org/10.1083/jcb.201812106

Figure 10. Model of SNX3-dependent processing of borreliae by macrophages. *B. burgdorferi* is internalized by macrophages through uptake into Rab22a-decorated phagosomes that are contacted by Rab5a vesicles that also contain SNX3. SNX3 enables docking of Rab5a vesicles to phagosomes by binding to PI(3)P on the phagosomal surface, which is enriched at sites of high curvature due to the helical shape of the spirochete. SNX3 also recruits, by its C-terminal region, a second subset of vesicles positive for galectin-9. Both Rab5a and galectin-9 contribute to phagosome compaction and phagolysosome maturation, leading to the elimination of spirochetes by human macrophages. PM, plasma membrane.

introducing two consecutive point mutations with oligonucleotides P11 and P12. siRNA-insensitive GFP-SNX3 and GFP-SNX3-Y71A were generated by introducing three single point mutations with P13 and P14 using same method. For details on mutagenesis primers, see Table S2.

Cloning of GST-fused SNX3 constructs

For recombinant expression of GST-fused SNX3 proteins, generation of respective plasmids was performed by PCR using P15 and P16 as primers and GFP-SNX3 and GFP-SNX3-Y71A as templates. PCR products were cloned into pGEX-2T (Invitrogen) using BamHI and EcoRI restriction sites. For detailed information on oligonucleotides, see Table S2.

Generation of GFP-Gal9 constructs, including deletion mutants, CRD mutants, and siRNA-insensitive mutants

GFP-Gal9 was cloned into pEGFP-C1 by amplifying Gal9 cDNA with oligonucleotides P09 and P10 using galectin-9 human–tagged ORF clone (GenBank accession number NM_009587) in pCMV-AC-TurboGFP (OriGene) as a template and XhoI and KpnI as restriction sites. Based on this full-length construct, five deletion constructs were generated by PCR and cloned into pEGFP vector using the same restriction enzymes. The following primers were used: P09+P22 for GFP-Gal9-ΔCRD2, P19+P10 for GFP-Gal9-ΔN, P21+P10 for GFP-Gal9-linker+CRD2, P09+P20 for GFP-Gal9-N+CRD1, and P19+P22 for GFP-Gal9-CRD1+linker. siRNA-insensitive GFP-Gal9 constructs were generated by introducing three single point mutations to all constructs except GFP-Gal9-linker+CRD2 with P23 and P24 using QuikChange Site-Directed Mutagenesis PCR (Agilent). For CRD mutants, three different amino acids were changed in siRNA-insensitive GFP-Gal9 by introducing one or two consecutive point mutations with oligonucleotides P25 and P26 for A46V, P27 and P28 for N137A, and P29 and P30 for R252A using same method. Double CRD1 mutant (GFP-Gal9-A46V+N137A) was generated by

a second change of amino acid N137A in the GFP-Gal9-A46V construct. For details on PCR primers, see Table S2.

Recombinant protein expression and purification

All GST constructs (GST alone, GST-WTSNX3, and GST-SNX3-Y71A) were expressed in L-arabinose–inducible *E. coli* BL21 as GST-fusion proteins. Expressed GST-fusion proteins from *E. coli* lysates were purified by affinity chromatography using immobilized glutathione-Sepharose 4B (GE Healthcare). Resulting eluates were dialyzed against DPBS overnight and purity was tested with SDS-PAGE and Coomassie Blue G-250 staining. Successful expression was confirmed with SDS-PAGE, Western blotting, and immunochemical staining with SNX3- and GST-specific antibodies.

Western blotting and immunochemical staining

Transfer of proteins from SDS gels onto nitrocellulose membrane was done with iBlot2 (Invitrogen) for 7 min at 20 V (program P3). The membrane was blocked subsequently in 5% skim milk/TBS-T (TBS buffer containing 0.3% Tween-20), incubated in primary antibody solution (5% BSA/TBS-T) for 60 min overnight, washed briefly with TBS-T, and incubated with secondary antibody (HRP-linked) solution (5% skim milk/TBS-T) for 60 min. SuperSignal West Pico or Femto Chemiluminescent Substrate (Thermo Scientific) was used for detection.

Cell transfection and siRNA experiments

Macrophages were transiently transfected with plasmid DNA using the Neon Transfection System (Life Technologies) with the following settings: pulse voltage, 1,000 V; pulse width, 40 ms; and pulse number, 2. Cells were transfected at a ratio of 10^5 cells to 0.5 μg DNA in R-buffer. Transfection of macrophages with siRNA (100 nM final concentration) was done with Viromer BLUE (Lipocalyx) according to the manufacturer's instructions for a 6-well multiwell plate type. Primary human

Klose et al.
SNX3 drives maturation of *Borrelia* phagosomes

Journal of Cell Biology 3055
https://doi.org/10.1083/jcb.201812106

macrophages were transfected with SNX1- and SNX3-specific siRNA once and with Gal9-specific siRNA twice at 0 and 48 h, and all cells were evaluated after a final incubation period of 70–72 h. For detailed information on siRNA sequences, see Table S2.

Phagocytosis assays

6- to 7-d-old macrophages were infected with borreliae at an MOI 100:1 in RPMI 1640 at 37°C for 1 h before immunofluorescence staining.

Intracellular survival assay

Macrophages were treated with specific siRNA for 72 h and infected with borreliae at an MOI of 100:1 in RPMI. After incubation at 37°C for 1 h, cells were washed five times with DPBS and warm RPMI was added to cells, supplemented with 300 µg/ml kanamycin and gentamicin to kill extracellular bacteria. Samples were incubated for 1 h with antibiotics at 37°C and washed 10 times with DPBS afterward. 400 µl DPBS was added to samples and transferred to 3.6 ml BSK-H medium (Sigma-Aldrich) containing 6% rabbit serum (Bio&Sell). No bacteria growth was observed in control samples. 400 µl DPBS was added to samples, which were lysed mechanically using a cell scraper, transferred in a 1.5-ml reaction tube, and centrifuged at 12,000 rpm for 8 min to disrupt remaining macrophages. To recover viable borreliae from the pellet, the pellet was resuspended in the supernatant and transferred to a 15-ml reaction tube containing 3.6 ml BSK-H medium with 6% rabbit serum and cultivated under microaerophilic conditions at 33°C and 1% CO_2. The number of borreliae was determined from day 7 to day 10 in a disposable C-Chip Neubauer improved hemocytometer (Biochrom) by dark-field microscopy with a Standard WL Upright Microscope, equipped with a central field stop, a Neofluar 163 NA 0.40/Ph2 objective lens, and two KF310/18 mm oculars (Zeiss).

DQ-BSA assay

$2 × 10^5$ macrophages were seeded on a 35-mm dish within the area of the 22-mm glass coverslip in the center of the dish (WillCo Wells). Cells were preincubated with 12.5 µg/ml Red DQ-BSA (DQ-BSA) for 1 h at 37°C (Life Technologies) in macrophage cultivation medium. GFP-borreliae were centrifuged, resuspended in RPMI supplemented with 12.5 µg/ml DQ-BSA, added to macrophages at an MOI 10:1, and incubated for 1 h at 37°C. Samples were washed three times with PBS, incubated for 1 h with 12.5 µg/ml DQ-BSA in RPMI at 37°C, washed again three times with PBS, and fixed for 10 min using 4% MeOH-free formaldehyde in PBS. For the DQ-BSA control assay, macrophages were treated as described above without infecting them. Images were acquired on an eclipse Ti spinning disk confocal microscope (Nikon) using a 40× CFI Plan Fluor Oil NA 1.3 immersion objective at a pixel resolution of 512 × 512. Image acquisition was performed using VisiView 3.0 Software (Visitron Systems), and analysis was performed using Volocity Software 6.1 (PerkinElmer); pixel mean intensity measurements were displayed using the plug-in for finding, measuring, and analyzing. For comparability, laser intensities (5% both green and

red fluorescence channel), exposure times (200 ms green and 150 ms red fluorescence channel), gains (400 both green and red fluorescence channels), and distance between confocal planes (0.3 µm) were not changed between measurements and experiments. For each value, 3 × 30 cells were evaluated.

Protein-lipid overlay assay

Hydrophobic membranes (PIP strips; Echelon Biosciences) spotted with 100 pmol of eight phosphoinositides and seven other biological important lipids were blocked with 3% BSA in PBS-T (PBS buffer containing 0.1% Tween-20) and subsequently incubated with recombinant GST-SNX3 and GST-SNX3-Y71A at a final concentration of 1 µg/ml diluted in fresh blocking buffer. Recombinant GST was used as a negative control. Detection of bound protein was done by immunochemical staining with SNX3- and GST-specific antibodies.

Immunoprecipitation

Immunoprecipitation of GFP constructs was performed according to the manufacturer's instructions (Miltenyi Biotec) with modifications. After transient transfection of macrophages with GFP constructs and pEGFP-C1 empty vector (control), cells were infected with borreliae at an MOI of 100:1 as described above. Cells were then washed twice with PBS and scraped from dishes in lysis buffer (50 mM Hepes, 150 mM NaCl, and 0.5% CHAPS, pH 7.5, with protease inhibitors; Roche) and collected in 1.5-ml reaction tubes. After a 10-min incubation on ice, samples were centrifuged at 10,000 ×g and 4°C for 15 min followed by collecting supernatants and protein concentration measurement with Pierce BCA assay (Thermo Scientific). Equal amounts of protein samples were incubated with µMACS anti-GFP microbeads overnight rotating at 4°C. After incubation, protein samples were loaded onto preequilibrated µMACS columns and washed twice with lysis buffer and once with 20 mM Tris-HCl (pH 7.5) before elution with buffer (50 mM Tris-HCl, pH 6.8, 50 mM DTT, 1% SDS, 0.005% bromphenol blue, and 10% glycerol). Samples were then mixed with 5× Laemmli SDS loading buffer, heated for 10 min at 95°C, and examined by SDS-PAGE, Western blot, and immunochemical staining.

Immunofluorescence and microscopy

Macrophages were seeded at a density of 10^5 cells per glass coverslip (12-mm diameter) and fixed for 10 min in 3.7% formaldehyde, washed three times in PBS, and permeabilized for 10 min in PBS containing 0.1% TritonX-100. After three washes with PBS, cells were incubated for 30 min in blocking solution (2% BSA or 2% normal human serum in PBS), washed briefly in PBS, and incubated for 60 min in the primary antibody solution. Cells were washed three times in PBS and then incubated for 30 min in secondary antibody solution. After three washes in PBS, coverslips were mounted on glass slides with Mowiol 4–88 (Roth) containing p-phenylenediamine (Sigma-Aldrich). Images of fixed samples were acquired with a confocal laser-scanning microscope (Leica DMi8 with a TCS SP8 AOBS confocal point scanner) equipped with an oil-immersion 63× HC PL APO Oil CS2 NA 1.40 objective and Leica LAS X SP8 software.

Klose et al.
SNX3 drives maturation of *Borrelia* phagosomes

Journal of Cell Biology   3056
https://doi.org/10.1083/jcb.201812106

Live-cell imaging

Cells were seeded on 18-mm glass coverslips at a density of 2×10^5, mounted in a 35-mm Chamlide CMB1 well magnetic chamber (Live Cell Instruments), and imaged in RPMI 1640 medium at 37°C. Images were acquired with a spinning disk confocal system (spinning disc CSU22) fitted on an eclipse Ti microscope (Nikon) with an oil-immersion 60× Apo total internal reflection fluorescence correction Oil NA 1.49 and 100× CFI Plan Apo Lambda NA 1.45 objective and a charge-coupled device camera (EM-CCD C-9100-2). Acquisition of images was performed using VisiView 3.0 Software (Visitron Systems), and processing of images was performed with Volocity Software 6.1 (PerkinElmer).

Mass spectrometry

Protein identification via analysis of the tryptic peptides by liquid chromatography–tandem mass spectrometry (LC-MS/MS) was achieved by injection of the samples onto a nano-liquid chromatography system (Dionex UltiMate 3000 RSLCnano; Thermo Scientific) coupled via electrospray ionization to a mass spectrometer equipped with a quadrupole, a linear trap, and an orbitrap (Orbitrap Fusion; Thermo Scientific) or with nano liquid chromatography system (nanoACQUITY; Waters) coupled via electrospray ionization to a mass spectrometer consisting of a quadrupole and an orbitrap mass analyzer (Orbitrap QExactive; Thermo Scientific). The resulting LC-MS/MS data were processed and analyzed with Proteome Discoverer 2.0 (Thermo Scientific). Identification of the proteins from the MS/MS spectra were performed with the search engine Sequest HT using the human SwissProt database (https://www.uniprot.org) and a contaminant database.

Statistical analysis

Statistical evaluation of datasets was performed using a two-tailed Student's t test and one-way ANOVA in GraphPad Prism 5.04 (GraphPad Software). For ANOVA, normality was tested by a D'Agostino and Pearson omnibus normality test and Shapiro–Wilk normality test. For Student's t tests, data distribution was assumed to be normal, but this was not formally tested. Statistically significant differences are indicated by asterisks (****, $P < 0.0001$; ***, $P < 0.001$; **, $P < 0.01$; and *, $P < 0.05$). Extreme outlier values for experiments described in Fig. 9 have been identified and removed according to an outlier analysis (Hoaglin et al., 1986). Briefly, this analysis identifies outlier values using the lower and upper quartiles F_L and F_U, according to the formula $F_U + 1.5(F_U - F_L)$.

Online supplemental material

Fig. S1 shows localization of SNX isoforms in macrophages with internalized borreliae. Fig. S2 shows localization of endogenous SNX1 and SNX3 at borreliae-containing phagosomes. Fig. S3 shows Western blots and evaluation of siRNA-mediated knockdown of SNX1 and SNX3. Fig. S4 shows localization of several phosphoinositols at *B. burgdorferi*–containing phagosomes. Fig. S5 shows gradual PI(3)P enrichment at borreliae phagosomes and occasional contact by PI(3)P- and Rab5a-positive vesicles. Fig. S6 shows a list and micrographs of potential SNX3 interaction partners. Fig. S7 shows a list and micrographs of potential galectin-9 interaction partners, as well as intracellular localization of various galectin-9 deletion constructs. Table S1 lists values for parameters following experimental treatments. Table S2 lists oligonucleotides, plasmids, and antibodies used in this study. Video 1 shows endogenous SNX3 enrichment at borreliae phagosomes. Video 2 shows enrichment of RFP-SNX3 during compaction of borreliae phagosomes. Video 3 shows localization of GFP-SNX3 to RFP-Rab5a–positive vesicles. Video 4 shows localization of GFP-galectin-9 to vesicles that contact a *B. burgdorferi*–containing phagosome. Video 5 shows gradual PI(3)P enrichment at borreliae phagosomes. Video 6 shows gradual PI(3)P enrichment at borreliae phagosomes and occasional contact by PI(3)P- and Rab5a-positive vesicles.

References

Aberer, E., and P.H. Duray. 1991. Morphology of Borrelia burgdorferi: structural patterns of cultured borreliae in relation to staining methods. *J. Clin. Microbiol.* 29:764–772.

Benach, J.L., H.B. Fleit, G.S. Habicht, J.L. Coleman, E.M. Bosler, and B.P. Lane. 1984. Interactions of phagocytes with the Lyme disease spirochete: role of the Fc receptor. *J. Infect. Dis.* 150:497–507. https://doi.org/10.1093/infdis/150.4.497

Bendris, N., and S.L. Schmid. 2017. Endocytosis, Metastasis and Beyond: Multiple Facets of SNX9. *Trends Cell Biol.* 27:189–200. https://doi.org/10.1016/j.tcb.2016.11.001

Böttcher, R.T., C. Stremmel, A. Meves, H. Meyer, M. Widmaier, H.Y. Tseng, and R. Fässler. 2012. Sorting nexin 17 prevents lysosomal degradation of β1 integrins by binding to the β1-integrin tail. *Nat. Cell Biol.* 14:584–592. https://doi.org/10.1038/ncb2501

Braun, V., A. Wong, M. Landekic, W.J. Hong, S. Grinstein, and J.H. Brumell. 2010. Sorting nexin 3 (SNX3) is a component of a tubular endosomal network induced by Salmonella and involved in maturation of the Salmonella-containing vacuole. *Cell. Microbiol.* 12:1352–1367. https://doi.org/10.1111/j.1462-5822.2010.01476.x

Bujny, M.V., P.A. Ewels, S. Humphrey, N. Attar, M.A. Jepson, and P.J. Cullen. 2008. Sorting nexin-1 defines an early phase of Salmonella-containing vacuole-remodeling during Salmonella infection. *J. Cell Sci.* 121: 2027–2036. https://doi.org/10.1242/jcs.018432

Burgdorfer, W., A.G. Barbour, S.F. Hayes, J.L. Benach, E. Grunwaldt, and J.P. Davis. 1982. Lyme disease-a tick-borne spirochetosis? *Science.* 216: 1317–1319. https://doi.org/10.1126/science.7043737

Carlton, J., M. Bujny, A. Rutherford, and P. Cullen. 2005. Sorting nexins--unifying trends and new perspectives. *Traffic.* 6:75–82. https://doi.org/10.1111/j.1600-0854.2005.00260.x

Chua, R.Y., and S.H. Wong. 2013. SNX3 recruits to phagosomes and negatively regulates phagocytosis in dendritic cells. *Immunology.* 139:30–47. https://doi.org/10.1111/imm.12051

Cinco, M., R. Murgia, G. Presani, and S. Perticarari. 1997. Integrin CR3 mediates the binding of nonspecifically opsonized Borrelia burgdorferi to human phagocytes and mammalian cells. *Infect. Immun.* 65:4784–4789.

Cozier, G.E., J. Carlton, A.H. McGregor, P.A. Gleeson, R.D. Teasdale, H. Mellor, and P.J. Cullen. 2002. The phox homology (PX) domain-dependent, 3-phosphoinositide-mediated association of sorting nexin-1 with an early sorting endosomal compartment is required for its ability to regulate epidermal growth factor receptor degradation. *J. Biol. Chem.* 277:48730–48736. https://doi.org/10.1074/jbc.M206986200

Cullen, P.J., and H.C. Korswagen. 2011. Sorting nexins provide diversity for retromer-dependent trafficking events. *Nat. Cell Biol.* 14:29–37. https://doi.org/10.1038/ncb2374

Daste, F., A. Walrant, M.R. Holst, J.R. Gadsby, J. Mason, J.E. Lee, D. Brook, M. Mettlen, E. Larsson, S.F. Lee, et al. 2017. Control of actin polymerization via the coincidence of phosphoinositides and high membrane curvature. *J. Cell Biol.* 216:3745–3765. https://doi.org/10.1083/jcb.201704061

Delacour, D., A. Koch, and R. Jacob. 2009. The role of galectins in protein trafficking. *Traffic.* 10:1405–1413. https://doi.org/10.1111/j.1600-0854.2009.00960.x

Ehsani, S., J.C. Santos, C.D. Rodrigues, R. Henriques, L. Audry, C. Zimmer, P. Sansonetti, G. Tran Van Nhieu, and J. Enninga. 2012. Hierarchies of host factor dynamics at the entry site of Shigella flexneri during host cell invasion. *Infect. Immun.* 80:2548–2557. https://doi.org/10.1128/IAI.06391-11

Elwell, C.A., N. Czudnochowski, J. von Dollen, J.R. Johnson, R. Nakagawa, K. Mirrashidi, N.J. Krogan, J.N. Engel, and O.S. Rosenberg. 2017. *Chlamydia* interfere with an interaction between the mannose-6-phosphate receptor and sorting nexins to counteract host restriction. *eLife.* 6:e22709. https://doi.org/10.7554/eLife.22709

Gallop, J.L., A. Walrant, L.C. Cantley, and M.W. Kirschner. 2013. Phosphoinositides and membrane curvature switch the mode of actin polymerization via selective recruitment of toca-1 and Snx9. *Proc. Natl. Acad. Sci. USA.* 110:7193–7198. https://doi.org/10.1073/pnas.1305286110

Gozani, O., P. Karuman, D.R. Jones, D. Ivanov, J. Cha, A.A. Lugovskoy, C.L. Baird, H. Zhu, S.J. Field, S.L. Lessnick, et al. 2003. The PHD finger of the chromatin-associated protein ING2 functions as a nuclear phosphoinositide receptor. *Cell.* 114:99–111. https://doi.org/10.1016/S0092-8674(03)00480-X

Haft, C.R., M. de la Luz Sierra, V.A. Barr, D.H. Haft, and S.I. Taylor. 1998. Identification of a family of sorting nexin molecules and characterization of their association with receptors. *Mol. Cell. Biol.* 18:7278–7287. https://doi.org/10.1128/MCB.18.12.7278

Hammond, G.R., M.P. Machner, and T. Balla. 2014. A novel probe for phosphatidylinositol 4-phosphate reveals multiple pools beyond the Golgi. *J. Cell Biol.* 205:113–126. https://doi.org/10.1083/jcb.201312072

Hammond, G.R., S. Takasuga, T. Sasaki, and T. Balla. 2015. The ML1Nx2 Phosphatidylinositol 3,5-Bisphosphate Probe Shows Poor Selectivity in Cells. *PLoS One.* 10:e0139957. https://doi.org/10.1371/journal.pone.0139957

Hawley, K.L., C.M. Olson Jr., J.M. Iglesias-Pedraz, N. Navasa, J.L. Cervantes, M.J. Caimano, H. Izadi, R.R. Ingalls, U. Pal, J.C. Salazar, et al. 2012. CD14 cooperates with complement receptor 3 to mediate MyD88-independent phagocytosis of Borrelia burgdorferi. *Proc. Natl. Acad. Sci. USA.* 109: 1228–1232. https://doi.org/10.1073/pnas.1112078109

Hoaglin, D.C., B. Iglewicz, and J.W. Tukey. 1986. Performance of Some Resistant Rules for Outlier Labeling. *J. Am. Stat. Assoc.* 81:991–999. https://doi.org/10.1080/01621459.1986.10478363

Hoffmann, A.K., X. Naj, and S. Linder. 2014. Daam1 is a regulator of filopodia formation and phagocytic uptake of Borrelia burgdorferi by primary human macrophages. *FASEB J.* 28:3075–3089. https://doi.org/10.1096/fj.13-247049

Hübner, S., A.D. Couvillon, J.A. Käs, V.A. Bankaitis, R. Vegners, C.L. Carpenter, and P.A. Janmey. 1998. Enhancement of phosphoinositide 3-kinase (PI 3-kinase) activity by membrane curvature and inositol-phospholipid-binding peptides. *Eur. J. Biochem.* 258:846–853. https://doi.org/10.1046/j.1432-1327.1998.2580846.x

Jia, J., Y.P. Abudu, A. Claude-Taupin, Y. Gu, S. Kumar, S.W. Choi, R. Peters, M.H. Mudd, L. Allers, M. Salemi, et al. 2018. Galectins Control mTOR in Response to Endomembrane Damage. *Mol. Cell.* 70:120–135.e128.

Johannes, L., C. Wunder, and M. Shafaq-Zadah. 2016. Glycolipids and Lectins in Endocytic Uptake Processes. *J. Mol. Biol.*: 428:4792–4818.

Johannes, L., R. Jacob, and H. Leffler. 2018. Galectins at a glance. *J. Cell Sci.* 131: jcs208884. https://doi.org/10.1242/jcs.208884

Kanai, F., H. Liu, S.J. Field, H. Akbary, T. Matsuo, G.E. Brown, L.C. Cantley, and M.B. Yaffe. 2001. The PX domains of p47phox and p40phox bind to lipid products of PI(3)K. *Nat. Cell Biol.* 3:675–678. https://doi.org/10.1038/35083070

Kimber, W.A., L. Trinkle-Mulcahy, P.C. Cheung, M. Deak, L.J. Marsden, A. Kieloch, S. Watt, R.T. Javier, A. Gray, C.P. Downes, et al. 2002. Evidence that the tandem-pleckstrin-homology-domain-containing protein TAPP1 interacts with Ptd(3,4)P2 and the multi-PDZ-domain-containing protein MUPP1 in vivo. *Biochem. J.* 361:525–536. https://doi.org/10.1042/bj3610525

Lakshminarayan, R., C. Wunder, U. Becken, M.T. Howes, C. Benzing, S. Arumugam, S. Sales, N. Ariotti, V. Chambon, C. Lamaze, et al. 2014. Galectin-3 drives glycosphingolipid-dependent biogenesis of clathrin-independent carriers. *Nat. Cell Biol.* 16:595–606. https://doi.org/10.1038/ncb2970

Lane, R.S., and J.E. Loye. 1991. Lyme disease in California: interrelationship of ixodid ticks (Acari), rodents, and Borrelia burgdorferi. *J. Med. Entomol.* 28:719–725. https://doi.org/10.1093/jmedent/28.5.719

Lee, S.H., J.S. Miller, J.J. Moon, and J.L. West. 2005. Proteolytically degradable hydrogels with a fluorogenic substrate for studies of cellular proteolytic activity and migration. *Biotechnol. Prog.* 21:1736–1741. https://doi.org/10.1021/bp0502429

Lou, J., X. Li, W. Huang, J. Liang, M. Zheng, T. Xu, J. Lyu, D. Li, Q. Xu, X. Jin, et al. 2017. SNX10 promotes phagosome maturation in macrophages and protects mice against *Listeria monocytogenes* infection. *Oncotarget.* 8: 53935–53947. https://doi.org/10.18632/oncotarget.19644

Lucas, M., D.C. Gershlick, A. Vidaurrazaga, A.L. Rojas, J.S. Bonifacino, and A. Hierro. 2016. Structural Mechanism for Cargo Recognition by the Retromer Complex. *Cell.* 167:1623–1635.

Marat, A.L., and V. Haucke. 2016. Phosphatidylinositol 3-phosphates-at the interface between cell signalling and membrane traffic. *EMBO J.* 35: 561–579. https://doi.org/10.15252/embj.201593564

McGough, I.J., R.E.A. de Groot, A.P. Jellett, M.C. Betist, K.C. Varandas, C.M. Danson, K.J. Heesom, H.C. Korswagen, and P.J. Cullen. 2018. SNX3-retromer requires an evolutionary conserved MON2:DOPEY2:ATP9A complex to mediate Wntless sorting and Wnt secretion. *Nat. Commun.* 9: 3737. https://doi.org/10.1038/s41467-018-06114-3

Meister, M., and R. Tikkanen. 2014. Endocytic trafficking of membrane-bound cargo: a flotillin point of view. *Membranes (Basel).* 4:356–371. https://doi.org/10.3390/membranes4030356

Mizutani, R., J. Yamauchi, S. Kusakawa, K. Nakamura, A. Sanbe, T. Torii, Y. Miyamoto, and A. Tanoue. 2009. Sorting nexin 3, a protein upregulated by lithium, contains a novel phosphatidylinositol-binding sequence and mediates neurite outgrowth in N1E-115 cells. *Cell. Signal.* 21:1586–1594. https://doi.org/10.1016/j.cellsig.2009.06.005

Montgomery, R.R., M.H. Nathanson, and S.E. Malawista. 1994. Fc- and non-Fc-mediated phagocytosis of Borrelia burgdorferi by macrophages. *J. Infect. Dis.* 170:890–893. https://doi.org/10.1093/infdis/170.4.890

Nagae, M., N. Nishi, S. Nakamura-Tsuruta, J. Hirabayashi, S. Wakatsuki, and R. Kato. 2008. Structural analysis of the human galectin-9 N-terminal carbohydrate recognition domain reveals unexpected properties that differ from the mouse orthologue. *J. Mol. Biol.* 375:119–135. https://doi.org/10.1016/j.jmb.2007.09.060

Nagae, M., N. Nishi, T. Murata, T. Usui, T. Nakamura, S. Wakatsuki, and R. Kato. 2009. Structural analysis of the recognition mechanism of poly-N-acetyllactosamine by the human galectin-9 N-terminal carbohydrate recognition domain. *Glycobiology.* 19:112–117. https://doi.org/10.1093/glycob/cwn121

Naj, X., and S. Linder. 2015. ER-Coordinated Activities of Rab22a and Rab5a Drive Phagosomal Compaction and Intracellular Processing of Borrelia burgdorferi by Macrophages. *Cell Reports.* 12:1816–1830. https://doi.org/10.1016/j.celrep.2015.08.027

Naj, X., and S. Linder. 2017. Actin-Dependent Regulation of Borrelia burgdorferi Phagocytosis by Macrophages. *Curr. Top. Microbiol. Immunol.* 399:133–154.

Naj, X., A.K. Hoffmann, M. Himmel, and S. Linder. 2013. The formins FMNL1 and mDia1 regulate coiling phagocytosis of Borrelia burgdorferi by primary human macrophages. *Infect. Immun.* 81:1683–1695. https://doi.org/10.1128/IAI.01411-12

Paul, B., H.S. Kim, M.C. Kerr, W.M. Huston, R.D. Teasdale, and B.M. Collins. 2017. Structural basis for the hijacking of endosomal sorting nexin proteins by *Chlamydia trachomatis*. *eLife.* 6:e22311. https://doi.org/10.7554/eLife.22311

Paz, I., M. Sachse, N. Dupont, J. Mounier, C. Cederfur, J. Enninga, H. Leffler, F. Poirier, M.C. Prevost, F. Lafont, and P. Sansonetti. 2010. Galectin-3, a marker for vacuole lysis by invasive pathogens. *Cell. Microbiol.* 12:530–544. https://doi.org/10.1111/j.1462-5822.2009.01415.x

Planchon, D., E. Rios Morris, M. Genest, F. Comunale, S. Vacher, I. Bièche, E.V. Denisov, L.A. Tashireva, V.M. Perelmuter, S. Linder, et al. 2018. MT1-MMP targeting to endolysosomes is mediated by upregulation of flotillins. *J. Cell Sci.* 131:jcs218925. https://doi.org/10.1242/jcs.218925

Pons, V., P.P. Luyet, E. Morel, L. Abrami, F.G. van der Goot, R.G. Parton, and J. Gruenberg. 2008. Hrs and SNX3 functions in sorting and membrane invagination within multivesicular bodies. *PLoS Biol.* 6:e214. https://doi.org/10.1371/journal.pbio.0060214

Ponting, C.P. 1996. Novel domains in NADPH oxidase subunits, sorting nexins, and PtdIns 3-kinases: binding partners of SH3 domains? *Protein Sci.* 5:2353–2357. https://doi.org/10.1002/pro.5560051122

Rao, Y., M.G. Perna, B. Hofmann, V. Beier, and T. Wollert. 2016. The Atg1-kinase complex tethers Atg9-vesicles to initiate autophagy. *Nat. Commun.* 7:10338. https://doi.org/10.1038/ncomms10338

Rittig, M.G., G.R. Burmester, and A. Krause. 1998. Coiling phagocytosis: when the zipper jams, the cup is deformed. *Trends Microbiol.* 6:384–388. https://doi.org/10.1016/S0966-842X(98)01343-2

Sada-Ovalle, I., L. Chávez-Galán, L. Torre-Bouscoulet, L. Nava-Gamiño, L. Barrera, P. Jayaraman, M. Torres-Rojas, M.A. Salazar-Lezama, and S.M. Behar. 2012. The Tim3-galectin 9 pathway induces antibacterial activity in human macrophages infected with Mycobacterium tuberculosis. *J. Immunol.* 189:5896–5902. https://doi.org/10.4049/jimmunol.1200990

Salazar, J.C., S. Duhnam-Ems, C. La Vake, A.R. Cruz, M.W. Moore, M.J. Caimano, L. Velez-Climent, J. Shupe, W. Krueger, and J.D. Radolf. 2009. Activation of human monocytes by live Borrelia burgdorferi generates TLR2-dependent and -independent responses which include induction of IFN-beta. *PLoS Pathog.* 5:e1000444. https://doi.org/10.1371/journal.ppat.1000444

Sason, H., M. Milgrom, A.M. Weiss, N. Melamed-Book, T. Balla, S. Grinstein, S. Backert, I. Rosenshine, and B. Aroeti. 2009. Enteropathogenic Escherichia coli subverts phosphatidylinositol 4,5-bisphosphate and phosphatidylinositol 3,4,5-trisphosphate upon epithelial cell infection. *Mol. Biol. Cell.* 20:544–555. https://doi.org/10.1091/mbc.e08-05-0516

Shin, O.S., L.S. Miller, R.L. Modlin, S. Akira, S. Uematsu, and L.T. Hu. 2009. Downstream signals for MyD88-mediated phagocytosis of Borrelia burgdorferi can be initiated by TRIF and are dependent on PI3K. *J. Immunol.* 183:491–498. https://doi.org/10.4049/jimmunol.0900724

Simonsen, A., A.E. Wurmser, S.D. Emr, and H. Stenmark. 2001. The role of phosphoinositides in membrane transport. *Curr. Opin. Cell Biol.* 13:485–492. https://doi.org/10.1016/S0955-0674(00)00240-4

Solis, G.P., N. Hülsbusch, Y. Radon, V.L. Katanaev, H. Plattner, and C.A. Stuermer. 2013. Reggies/flotillins interact with Rab11a and SNX4 at the tubulovesicular recycling compartment and function in transferrin receptor and E-cadherin trafficking. *Mol. Biol. Cell.* 24:2689–2702. https://doi.org/10.1091/mbc.e12-12-0854

Steere, A.C., S.E. Malawista, D.R. Snydman, R.E. Shope, W.A. Andiman, M.R. Ross, and F.M. Steele. 1977. Lyme arthritis: an epidemic of oligoarticular arthritis in children and adults in three connecticut communities. *Arthritis Rheum.* 20:7–17. https://doi.org/10.1002/art.1780200102

Straube, T., T. von Mach, E. Hönig, C. Greb, D. Schneider, and R. Jacob. 2013. pH-dependent recycling of galectin-3 at the apical membrane of epithelial cells. *Traffic.* 14:1014–1027. https://doi.org/10.1111/tra.12086

Teasdale, R.D., D. Loci, F. Houghton, L. Karlsson, and P.A. Gleeson. 2001. A large family of endosome-localized proteins related to sorting nexin 1. *Biochem. J.* 358:7–16. https://doi.org/10.1042/bj3580007

Traer, C.J., A.C. Rutherford, K.J. Palmer, T. Wassmer, J. Oakley, N. Attar, J.G. Carlton, J. Kremerskothen, D.J. Stephens, and P.J. Cullen. 2007. SNX4 coordinates endosomal sorting of TfnR with dynein-mediated transport into the endocytic recycling compartment. *Nat. Cell Biol.* 9:1370–1380. https://doi.org/10.1038/ncb1656

Tseng, H.Y., N. Thorausch, T. Ziegler, A. Meves, R. Fässler, and R.T. Böttcher. 2014. Sorting nexin 31 binds multiple β integrin cytoplasmic domains and regulates β1 integrin surface levels and stability. *J. Mol. Biol.* 426:3180–3194. https://doi.org/10.1016/j.jmb.2014.07.003

Várnai, P., and T. Balla. 1998. Visualization of phosphoinositides that bind pleckstrin homology domains: calcium- and agonist-induced dynamic changes and relationship to myo-[3H]inositol-labeled phosphoinositide pools. *J. Cell Biol.* 143:501–510. https://doi.org/10.1083/jcb.143.2.501

Worby, C.A., and J.E. Dixon. 2002. Sorting out the cellular functions of sorting nexins. *Nat. Rev. Mol. Cell Biol.* 3:919–931. https://doi.org/10.1038/nrm974

Worby, C.A., N. Simonson-Leff, J.C. Clemens, R.P. Kruger, M. Muda, and J.E. Dixon. 2001. The sorting nexin, DSH3PX1, connects the axonal guidance receptor, Dscam, to the actin cytoskeleton. *J. Biol. Chem.* 276:41782–41789. https://doi.org/10.1074/jbc.M107080200

Xu, Y., H. Hortsman, L. Seet, S.H. Wong, and W. Hong. 2001. SNX3 regulates endosomal function through its PX-domain-mediated interaction with PtdIns(3)P. *Nat. Cell Biol.* 3:658–666. https://doi.org/10.1038/35083051

Yoshida, H., M. Teraoka, N. Nishi, S. Nakakita, T. Nakamura, M. Hirashima, and S. Kamitori. 2010. X-ray structures of human galectin-9 C-terminal domain in complexes with a biantennary oligosaccharide and sialyllactose. *J. Biol. Chem.* 285:36969–36976. https://doi.org/10.1074/jbc.M110.163402

Zajkowska, J., P. Lewczuk, F. Strle, and G. Stanek. 2012. Lyme borreliosis: from pathogenesis to diagnosis and treatment. *Clin. Dev. Immunol.* 2012:231657. https://doi.org/10.1155/2012/231657